Journal of Sedimentary Research

Journal of Sedimentary Research, 2020, v. 90, 1770–1801
Research Article
DOI: 10.2110/jsr.2020.75

TESTING HYPOTHESES ON SIGNATURES OF PRECIPITATION VARIABILITY IN THE RIVER AND FLOODPLAIN DEPOSITS OF THE PALEOGENE SAN JUAN BASIN, NEW MEXICO, U.S.A.

KRISTINE L. ZELLMAN,[1,2] PIRET PLINK-BJÖRKLUND,[2] AND HENRY C. FRICKE[3]
[1]U.S. Geological Survey, Geosciences and Environmental Change Science Center, Box 25046, DFC, MS 980, Denver, Colorado 80225, U.S.A.
[2]Colorado School of Mines, Geology and Geological Engineering, Golden, Colorado 80401, U.S.A.
[3]Colorado College, Department of Geology, Colorado Springs, Colorado 80903, U.S.A.
e-mail: kzellman@usgs.gov

ABSTRACT: **Much progress has been made in recent years towards a set of recognition criteria for river discharge variability in river channel deposits, and thus sedimentary proxies for precipitation variability. Despite this progress, there is currently no consensus on how different styles of discharge variability are reflected in river sedimentary records, and whether variable-discharge river records from different climate types can be distinguished. Herein, river discharge and precipitation variability in the Paleogene is investigated using associations between river channel and floodplain deposits across the Paleocene–Eocene boundary from the Paleocene upper Nacimiento Formation and the early Eocene San Jose Formation in the San Juan Basin, New Mexico, USA.**

The succession is identified as deposits of variable-discharge river systems based on shared channel-deposit characteristics with modern and ancient variable-discharge river systems and the proposed facies models, in addition to alternations of poorly drained and well-drained floodplain deposits and/or slickensides indicating alternating wet–dry cycles. A long-term stratigraphic trend toward increasingly well-drained floodplain deposits is also observed and hypothesized to indicate successively more arid conditions from the Paleocene into the early Eocene. Comparisons with modern rivers from various climate zones suggest a long-term shift from a monsoonal climate in the Paleocene, to a fluctuating subhumid climate, ultimately leading to semiarid to arid conditions in the early Eocene. These observations suggest that floodplain deposits may be a better indicator of ambient climate, whereas channel deposits are records for frequency and magnitude of high-intensity precipitation events. Therefore, the existing facies models for variable-discharge rivers that consider only channel facies may not capture critical information needed to make accurate interpretations of paleoclimatic conditions. This study also adds to a growing body of evidence from geologic records of mid-latitude Paleogene river systems suggesting increases in the magnitude or variability of river discharge coinciding with established climate perturbations.

INTRODUCTION

The surface of the Earth is shaped by tectonics and climate. Geomorphic and sedimentary records are archives of changes to these tectonic and climate regimes (e.g., Wobus et al. 2006a; Tucker 2009). To decipher the geomorphic or sedimentary record effectively and distinguish the tectonic and climatic signals, a sound understanding of how landscapes respond to changes in tectonic or climatic boundary conditions is required (e.g., Whittaker 2012). Such deductions are ambitious because climate, tectonics, and landscape are linked in a complex fashion and display nonlinear dynamics (e.g., Wobus et al. 2006a, 2006b; Whipple 2009; Jerolmack and Paola 2010; DiBiase and Whipple 2011). Deciphering climatic signals from landscape topography has been proven especially difficult due to nonunique and difficult to decode responses (Sólyom and Tucker 2004; Tucker 2004; Molnar et al. 2006; DiBiase and Whipple 2011). In some situations, therefore, the best archive of landscape response to past climate may be the sedimentary record (Allen 2008; Whittaker et al. 2009; Armitage et al. 2011; Whittaker 2012). Thus, clear recognition criteria are particularly needed regarding the expression of specific climate changes in the sedimentary record.

Climate, Precipitation, and River Discharge

Rivers are especially sensitive to tectonic and climatic forcing via their channel gradient and discharge (e.g., Bull 1991, 2009; Macklin et al. 2012; Whittaker 2012) that also affect the amount and composition of sediment (e.g., Cecil et al. 2003). Tectonic processes create topography and maintain relief through crustal uplift (Whipple 2004; Wobus et al. 2006a; Whittaker et al. 2008). Climate provides the water needed for vegetation growth, soil development, and runoff that facilitates sediment transport, and thus influences the flux of water (discharge) and sediment that ultimately makes it into a river system (Leeder 2011). Changes in climate can perturb these hydrological and sediment supply variables, thus altering erosion and sedimentation (e.g., Molnar et al. 2006).

Precipitation is one of the primary controls on river discharge and sediment yield (Langbein and Schumm 1958). While traditional approaches (e.g., Langbein and Schumm 1958) have focused on mean annual precipitation, and thus considered changes in humidity as the key aspect of climate control on river discharge and sediment yields (e.g., Syvitski and Milliman 2007), the temporal distribution of runoff plays a major role in determining stream-channel and floodplain sedimentary

Published Online: December 2020
 1527-1404/20/090-1770

processes through its control on the overall hydrology and the nature of river morphodynamics, sedimentary environments, and soil development (e.g., Cecil et al. 2003; Goodbred 2003; Latrubesse et al. 2005; Molnar et al. 2006; Powell 2009). Rivers subject to high variability in precipitation in their drainage areas also experience variable discharge (Latrubesse et al. 2005; Leier et al. 2005; Hansford et al. 2020). River discharge variability is a function of seasonal (intra-annual) as well as interannual variability (Hansford et al. 2020). Modern examples of variable-discharge rivers have been highlighted primarily in arid subtropics (dryland rivers) (e.g., Graf 1988; Knighton and Nanson 1997; Tooth 2000; Powell 2009; Reid and Frostick 2011), but are also recognized in the subhumid subtropics (e.g., Alexander et al. 1999a; Fielding et al. 2009, 2011) and monsoonal tropics (e.g., Latrubesse et al. 2005; Leier et al. 2005), and also in areas proximal to glaciers (e.g., Willis 2005).

Intense monsoon-driven summer rainfall causes high-magnitude flooding in rivers that transmit a relatively low base flow during a sustained dry season (Latrubesse et al. 2005; Fielding et al. 2009, 2011; Syvitski et al. 2014; Plink-Björklund 2015). As a result, these rivers are shown to deliver most of their water discharge and sediment load during the summer monsoon season (Goodbred 2003), because only the flood discharge is geomorphically effective and able to transport sediment (Henck et al. 2010; Plink-Björklund 2015). Exceptions include rivers that have part of their drainage in a different climate zone (e.g., the Nile). In the monsoon zone and in some subtropics, the intense monsoon-driven precipitation may occur seasonally. More characteristically, subtropical areas have high interannual variability with a precipitation recurrence frequency of multiple years or even decades, thus some subtropical rivers are ephemeral and may remain dry over these timescales (e.g., Alexander et al. 1999a). This extreme interannual precipitation variability is especially distinct in areas that receive monsoon rain only during extreme events. Interannual monsoon anomalies have been shown to intensify the precipitation extremes, resulting in catastrophic flooding events interspersed with droughts (Seneviratne et al. 2012; IPCC 2014). In addition, observations and proxy data have shown that monsoon intensity can also vary along longer time scales from interdecadal to millennial (Wang et al. 2014).

Fluvial Deposits as Archives of Past Climates

There has been significant progress towards deciphering the signal of discharge variability in river records and thus towards developing paleoclimate proxies for precipitation variability. This work has developed sedimentary proxies that highlight an abundance of upper-flow-regime (UFR) sedimentary structures as a key recognition criterion for river discharge variability (Tunbridge 1981; Sneh 1983; Stear 1985; Deluca and Eriksson 1989; North and Taylor 1996; Billi 2007; Fielding and Alexander 1996; Fielding et al. 1999, 2009, 2011, 2018; Fielding 2006; Allen et al. 2014; Plink-Björklund 2015). This abundance implies high flow velocities, and the characteristically rapid rise, sharp peak, and rapid decline of flows as seen on flood hydrographs. Fielding et al. (1999, 2009, 2011; see also Fielding and Alexander 1996) further highlighted in-channel vegetation and vegetation-induced sedimentary structures in addition to the abundance of UFR sedimentary structures and developed a facies model with recognition criteria for subhumid subtropical rivers through observations of the modern Burdekin River in Australia and rock-record analogues. Colonization of the channel floor by vegetation indicates periods of very low flow or lack of base flow, and a seasonally low water table that is more accessible from the channel floor, a condition most likely to occur in subhumid subtropics (Fielding et al. 2009, 2011; Allen et al. 2011, 2014). Furthermore, Fielding et al. (2011) documented changes in the style of fluvial deposits from the rock record in the Pennsylvanian of the Maritimes Basin Complex of Atlantic Canada which they interpret as recording a transition from perennial to subhumid to semiarid climatic conditions. They cite similarities with the modern Burdekin River deposits as evidence of deposition under subhumid to semiarid climatic conditions, whereas the underlying deposits contain a dominance of cross stratification suggesting a relatively sustained discharge regime characteristic of perennial river systems with low discharge variability. The change in channel-fill style is coincident with a gradual change in floodplain deposits from "drab" with carbonaceous plant debris, freshwater limestones, and carbonaceous shales to increasingly red with carbonate nodules, suggesting a shift from water-logged to well-drained conditions (Fielding et al. 2011). Plink-Björklund (2015) reviewed 17 modern and 35 ancient sedimentary records of variable-discharge rivers across the subtropics and the monsoon zone and suggested further recognition criteria, such as high-deposition-rate sedimentary structures, in-channel mud layers, thick soft-clast conglomerates, in-channel trace fossils, soft-sediment deformation, and the presence of flood event beds. Lack of bar forms or well-developed accretion sets, recognizable as point-bar or braid-bar strata, has been suggested as another key characteristic of rivers with variable discharge (e.g., Rhee and Chough 1993; Uba et al. 2005; Billi 2007; Hampton and Horton 2007; Fielding et al. 2009, 2011, 2018; Hulka and Heubeck 2010; Allen et al. 2011; Plink-Björklund 2015). However, Wang and Plink-Björklund (2020) document macroform or bar-scale architecture that they interpret as characteristic of variable-discharge rivers, including low-angle downstream accretion sets, channel-scale scour-and-fill structures, and erosionally bound channel-scale backsets. Plink-Björklund (2015) further observed that the sedimentary record of variable-discharge rivers exhibits considerable variability in the proportions of characteristic facies and architectural elements and attempted to link that variability to the presence of a wet season vs. erratic storm occurrence, as well as to the presence or absence of the base flow. A different approach was taken by Fielding et al. (2018), with a focus on the role of interannual peak discharge variability as a sole control on depositional style, based on an observation that modern rivers with similar interannual variability displayed similar styles of preserved sedimentology, even if the patterns of intra-annual variability were different. In contrast, analyses of global river discharge by Hansford et al. (2020) suggest that a significant divergence in the style of discharge variability is linked to both intra- and interannual variability, such as seasonal, erratic and single-storm-controlled behavior that all contrast with persistent discharge patterns. In summary, despite the progress towards recognition criteria for river discharge variability and thus sedimentary proxies for precipitation variability, there is currently no consensus on how different styles of discharge variability are reflected in river sedimentary records and whether records of variable-discharge rivers from different climate types can be distinguished.

Paleogene Climate Trends

Earth's climate has evolved dramatically over the past 60 million years. Complex fluctuations in thermal regimes have resulted in extremes ranging from hothouse climates with ice-free poles to icehouse climates with expansive continental ice sheets (e.g., Zachos et al. 2008). These climatic variations can take place gradually over millions of years driven by tectonic processes, they can be cyclic over tens to hundreds of thousands of years driven by orbital forcing, or they can occur as anomalous perturbations (Zachos 2001). Of particular interest are perturbations that took place during the Paleogene, which are characterized by global increases in temperature and are thus termed hyperthermal events (Kennett and Stott 1991). Some hyperthermal events are known to have caused severe climatic and biotic change in both marine and terrestrial environments (Gingerich 1989; Thomas 1989; Kennett and Stott 1991; Koch et al. 1992; McInerney and Wing 2011). It is also known that extreme climate fluctuations are likely to affect earth surface processes (Sólyom and Tucker 2004; Molnar et al. 2006; Tucker 2009; DiBiase and Whipple 2011). A growing body of evidence from mid-latitude Paleogene terrestrial datasets suggests climate-change-driven changes to river systems coinciding with

some of these hyperthermal events that is suggestive of an increase in the magnitude or variability of river discharge (Schmitz and Pujalte 2007; Foreman et al. 2012; Foreman 2014; Birgenheier et al. 2020; Wang and Plink-Björklund 2019). Additional datasets are needed to further the understanding of how these responses varied on regional and global scales and ultimately provide data for paleoclimate reconstructions.

Aims of This Study

The San Juan Basin in New Mexico (Fig. 1) preserves the southernmost sedimentary record of the Paleocene and early Eocene in North America, and thus represents a critical datapoint of comparison for climatic and biotic change during the Paleogene. This paper documents channel and floodplain facies and their depositional styles in the Paleogene San Juan Basin with the aim to 1) explore the differences in the depositional style of variable-discharge rivers and their corresponding floodplain deposits, 2) propose links between the depositional style of river deposits and climate, and 3) test previous hypotheses for variable-discharge-river facies models proposed by Fielding et al. (2009, 2011, 2018) and Plink-Björklund (2015, 2019) by combined examination of both channel and floodplain depositional characteristics. Ultimately, the goal of the study is to examine discharge variability at multiple scales and discuss the potential implications for improving our understanding of Paleocene–Eocene climates.

GEOLOGICAL SETTING AND BACKGROUND

The San Juan Basin is in the Four Corners region of northwestern New Mexico and southwestern Colorado and is one of several intraforeland basins formed during the Laramide orogeny (Dickinson et al. 1988; Cather 2004). Laramide tectonics during the Late Cretaceous through the Eocene caused subsidence of the San Juan Basin in response to uplift of surrounding areas (Cather 2004). Baltz (1967) and Pecha et al. (2018) suggested that the San Juan Basin received most of its sediments from highlands to the north and the early San Juan uplift, although source areas in the Brazos–Sangre de Cristo, Nacimiento, Zuni, and Defiance uplifts are also suspected (Smith 1992; Cather 2004; Pecha et al. 2018) (Fig. 1B). Long-term evolution of the Cretaceous–Eocene sedimentary succession has been linked to tectonic episodes of subsidence in response to the Laramide orogeny (Fassett 1985; Cather 2004). The intraformational angular unconformity and reverse faults evident from outcrops in the eastern part of the study area show that the Paleogene units in the San Juan Basin were deposited simultaneously with deformation along the basin-bounding Nacimiento fault (Woodward 1987; Smith 1988) (Fig. 1B).

Stratigraphy

The Paleogene units preserved in the San Juan Basin are the earliest Paleocene Ojo Alamo Sandstone (Toa), the Paleocene Nacimiento Formation (Tn), and the early Eocene San Jose Formation (Tsc, Tsr, and Tstl) (Fig. 1C, D). These units crop out in a series of badlands and cliff-forming sandstones along the western and southern part of the San Juan Basin. This study focuses on the uppermost Nacimiento Formation and the Cuba Mesa Member and Regina Member of the San Jose Formation.

Paleocene Nacimiento Formation.—The Paleocene Nacimiento Formation is composed primarily of fluvial deposits consisting of a succession of sandstones and varicolored mudrocks, and the formation has a thickness of as much as 525 m (Baltz 1967; Williamson and Lucas 1992). The Nacimiento Formation is divided by lithologic and sedimentologic features into three members: the Arroyo Chijuillita (oldest), the Ojo Encino, and the Escavada (youngest) (Williamson and Lucas 1992). The Arroyo Chijuillita Member is characterized by "drab" mudrocks and sparse heterolithic sandstones. The Ojo Encino Member is also dominantly mudrock and is characterized by repetitive black-red-green-white banding that is associated with variegated mudrocks (black, red, and green) and fine-grained sandstones (white) (Williamson and Lucas 1992). Three persistent black mudrock deposits in the Ojo Encino Member (referred to as the lower black, middle black, and upper black) can be correlated across the basin and serve as useful marker beds (see Leslie et al. 2018). The Escavada Member is characterized by a predominance of sandstones, "drab" mudrocks, and abundant silcretes (Williamson et al. 1992). Across the southern San Juan Basin, the thickness of the Escavada Member varies (19–88 m) due to intraformational thinning (Butler and Lindsay 1985) and channel scouring at the base of the San Jose Formation (Williamson and Lucas 1992). A north-to-south decrease in grain size and paleocurrent measurements indicate a prevailing north-to-south paleoflow throughout the Nacimiento Formation (Baltz 1967; Klute 1986; Sikkink 1987; Smith 1992). The early Paleocene ages of the Arroyo Chijuillita and Ojo Encino members of the Nacimiento Formation are well constrained by biostratigraphy, magnetostratigraphy, and radiometric dating (Williamson and Lucas 1992; Leslie et al. 2018). The age of the Escavada Member is poorly constrained, with the only age indicator being a zone of normal polarity in the western San Juan Basin that has been correlated to chron 26 (59.24–58.96 Ma), suggesting a late Paleocene age (Butler and Lindsay 1985).

Lower Eocene San Jose Formation.—The San Jose Formation is the most extensively preserved and exposed Eocene unit in New Mexico (Baltz 1967; Smith and Lucas 1991). Similar to the underlying Nacimiento Formation, it is composed of fluvial deposits. Previous geological investigations of the southern and southeastern outcrop areas of the San Jose Formation include descriptions of fossils and local stratigraphy (e.g., Simpson 1948; Lucas et al. 1981; Smith and Lucas 1991; Smith 1992) and regional mapping (Baltz 1967; Mytton 1983; Manley et al. 1987). The San Jose Formation contains both sandstone-dominated and mudrock-dominated lithofacies. The sandstone vs. mudrock dominance is the primary characteristic used to distinguish between the members in the San Jose Formation, which from oldest to youngest are the Cuba Mesa (sandstone dominant), Regina (mudrock dominant), Ditch Canyon (sandstone dominant), Llaves (sandstone dominant), and Tapicitos (mudrock dominant) (Baltz 1967; Smith 1992). The Cuba Mesa Member at the base of the San Jose Formation is a 25–240-m-thick (based on lithostratigraphy) succession that overlies the Paleocene Nacimiento Formation (Baltz 1967; Smith and Lucas 1991). It consists of medium- to very coarse-grained, buff-colored sheet sandstones that thicken locally in vertically stacked (amalgamated) channel belts that can attain thicknesses up to 100 m, with channel width-to-thickness ratios ranging from 20 to $>$ 1000 (Smith 1988). The basal sandstone of the Cuba Mesa Member is continuous, nearly basin wide, over an area of $\sim$ 8000 km^2 (Smith 1988). In some parts of the basin, the contact between the Nacimiento and Cuba Mesa Member of the San Jose Formation can be difficult to distinguish because the Escavada Member of the Nacimiento Formation contains arkosic sandstones that are similar in lithology to those of the Cuba Mesa Member (Baltz 1967; Smith and Lucas 1991). Like the underlying Escavada Member, no age-diagnostic fossils or dateable materials have been discovered, leaving the deposits of both the upper Nacimiento Formation and the lower San Jose Formation with uncertain age constraints. It has long been proposed that a large unconformity ($\geq$ 5.6 My; Fassett et al. 2010) separates the Nacimiento and San Jose Formations in the southern San Juan Basin only (Barnes et al. 1954; Stone 1983; Smith and Lucas 1991) or throughout the basin (Cather 2004). Due to the lack of age constraints in this interval and ongoing reinvestigation of the nature of the Nacimiento–San Jose contact, we have not identified the unconformity on our simplified stratigraphic column, and we show that the location of the boundary between Paleocene and Eocene deposits is uncertain (Fig. 1C).

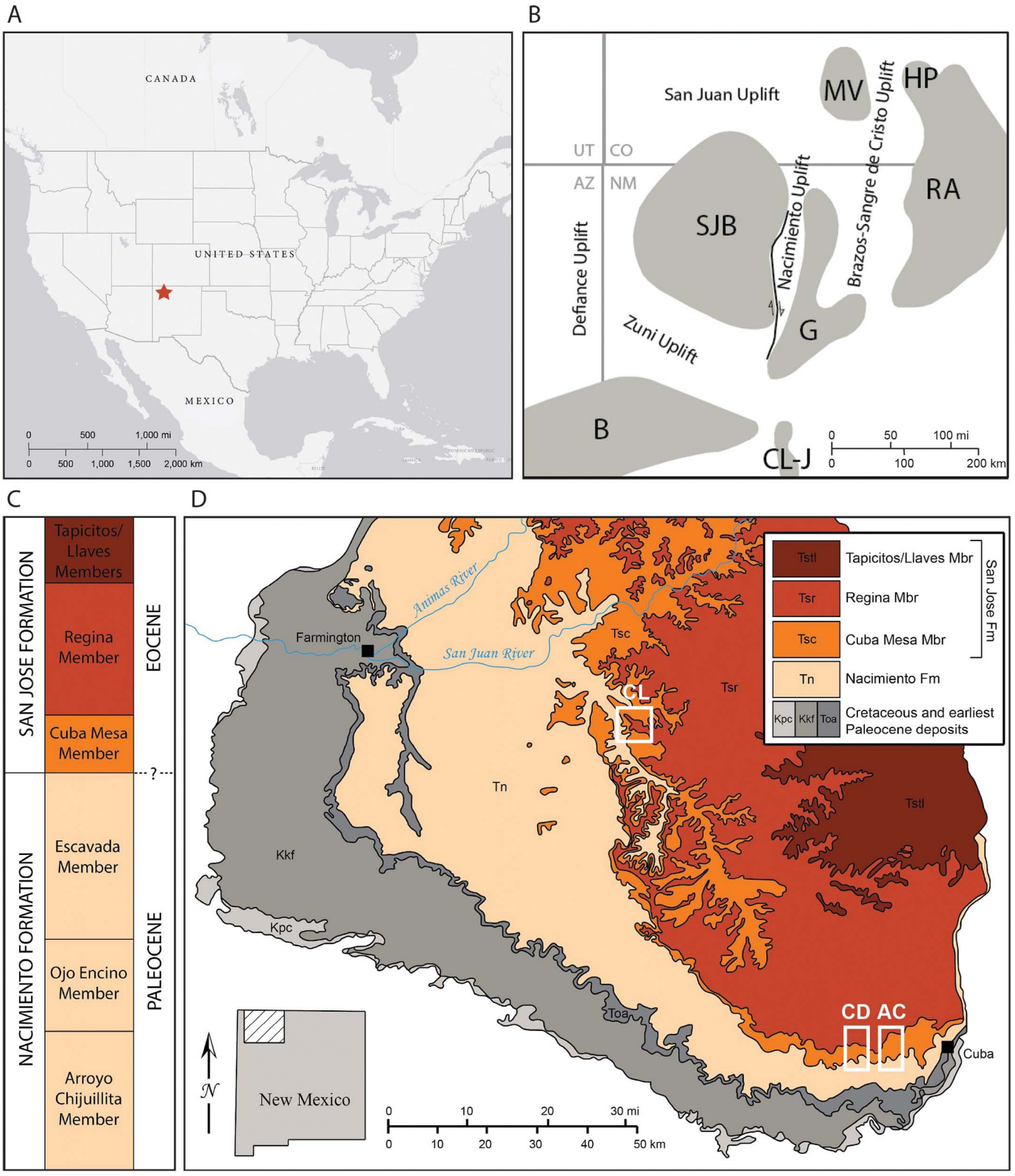

FIG. 1.—Regional maps and Paleogene stratigraphy of the San Juan Basin (SJB). **A)** Location of the San Juan Basin in the conterminous United States. **B)** Regional map of the San Juan Basin (SJB) and adjacent basins and uplifts (G, Galisteo Basin; B, Baca Basin; MV, Monte Vista Basin; RA, Raton Basin; HP, Huerfano Park Basin; CL-J, Carthage–LaJoya Basin). Redrawn from Dickinson et al. (1988), Lawton (2008), and Cather (2004). **C)** Simplified Paleogene stratigraphy of the SJB. **D)** Geologic map of the SJB and areas selected for detailed investigations. Arroyo Chijuilla (AC) and Continental Divide (CD) are in the southern SJB. Cañon Largo (CL) is in the central SJB. Map modified from Williamson et al. (2008) and Manley et al. (1987).

The Regina Member of the San Jose Formation ranges from 150 to 460 m in thickness and is composed of varicolored mudrock and interbedded sandstone. The sandstone beds are lenticular over spatial scales ranging from a few meters to many kilometers (Smith 1992). Lenticular conglomeratic sandstones in the northernmost outcrops of the member contain cobbles derived from Proterozoic rocks common in the San Juan uplift north of the San Juan Basin (Smith 1992). Vertebrate fossils from the Regina Member provide the only means by which the early Eocene age of the San Jose Formation has been determined (Williamson and Lucas 1992).

DATASET AND METHODS

For this study, detailed investigations were conducted in three locations with exposures of the upper Nacimiento Formation, Cuba Mesa Member, and Regina Member: Arroyo Chijuilla (AC) and Continental Divide (CD) in the southern San Juan Basin, and Cañon Largo (CL) in the central San Juan Basin (Fig. 1D). Approximately 720 m of section were measured between these three sites. Sandstones were described at 10 cm resolution based on bedsets, sedimentary structures, biogenic structures, and grain characteristics (size, shape, sorting, and composition). Mudrocks were described based on texture and color at 1–1.5 m resolution. We used a qualitative assessment of texture and color (e.g., Tabor et al. 2017) during this initial investigation in lieu of a detailed future paleopedological study. Rooting structures, burrows, soil structure (peds), and presence of nodules were noted on the measured section when they were apparent. Herein, mudrocks are identified as paleosols where visible evidence of pedogenesis is observed, such as mottling and ped structures. Mudrocks are identified as devoid of visible pedogenic modification where relict laminae or plant fragments are observed and indicate absent or minimal soil formation processes.

Photomosaics of outcrops were collected to document macroform characteristics and associations between sandstone and mudrock depositional styles. Sandstone channel thicknesses and widths were measured from outcrops in the Arroyo Chijuilla study area using a using a laser rangefinder mounted to a tripod. Laterally extensive channels were measured by collecting GPS coordinates at channel terminations. Sedimentary facies proportions were quantified using the measured facies thicknesses as compared to the total measured section thickness.

In an effort to characterize paleoclimatic conditions and their variability across the studied stratigraphic interval, comparisons to modern climate conditions were used by estimating the overall precipitation regime, rather than latitude. We utilize sedimentological signatures of precipitation variability (see Fielding 2006; Fielding et al. 2009, 2011; Plink-Björklund 2015) and paleosol characteristics (e.g., Kraus 1999; Tabor et al. 2017). We do not infer that the past conditions were comparable to every aspect of the modern climate types, but rather use this as a general illustration of paleoclimate conditions. Monsoon climate (Am in the Köppen–Geiger modern climate classification; see Peel et al. (2007)) is characterized by an annually high and a highly seasonal precipitation pattern, where the precipitation range (wet–dry season) is characteristically high due to the yearly migration of the Inter-Tropical Convergence Zone (ITCZ) (Wang and Ding 2008). Subhumid tropical climate types (Aw and As in the Köppen–Geiger modern climate classification; see Peel et al. (2007)) occur at an intermediate position between the ITCZ and the subtropical high-pressure cells, moving poleward. Like the monsoon climate, there is a distinct seasonality to precipitation, but with a much shorter and less sustained wet season and a considerably higher interannual variability (Wang and Ding 2008). In arid climate types (Bw and Bs in the Köppen–Geiger modern climate classification; see Peel et al. (2007)), mean annual precipitation is less than potential evapotranspiration and precipitation events are erratic and may have interannual to interdecadal return frequency. Arid climates thus have an extreme interannual precipitation variability, as they receive monsoon rain only during extreme monsoon trough migration or abnormal or strengthened monsoon seasons and associated cylconic flow. Following these definitions, we refer to paleoclimate conditions as monsoonal, if there is evidence for precipitation variability and a high soil moisture; as arid if there is evidence for precipitation variability and a low (well drained) soil moisture; and as subhumid if there is evidence for precipitation variability and a relatively low soil moisture but with indicators for less well-drained conditions than in the latter.

SEDIMENTARY FACIES AND FACIES ASSOCIATIONS

The studied succession consists of erosionally based lenticular or laterally and/or vertically amalgamated lithosomes, 2–50 m thick and 30–1500 m wide, that are dominated by sandstone facies (Tables 1, 2) and laterally associated and vertically interbedded with mudrock-dominated facies (Tables 3, 4). In sandstones, facies group 1 (Fig. 2, Table 1) is the most abundant, composing approximately 85% of all the sandstone facies present, and includes conglomerates (S1.1–14%), sandstones with scour-and-fill structures (S1.2–21%), sandstones with planar to low-angle laminae (S1.3–19%), sandstones with convex-up, long-wavelength laminae (S1.4–8%), sandstones with soft-sediment deformation (S1.5–5%), and structureless sandstones (S1.6–18%) (Fig. 2, Table 1). Commonly, these facies transition vertically and/or laterally into one another, forming complex relations when viewed in outcrop (Fig. 3). Sandstone facies group 2 (Fig. 4; Table 2) consists of sandstones with cross strata and laminae at or close to the angle of repose and form consistent cross sets. This facies group composes approximately 15% of the sandstone facies and includes cross-stratified sandstones (S2.1–11%), sandstones with climbing cross strata (S2.2–0.1%), sandstones with scours and climbing cross laminae (S2.3–2%), and sandstones with overturned cross strata or laminae (S2.4–2%). Sandstone facies group 1 is interpreted as upper-flow-regime (UFR) and high-deposition-rate (HDR) deposits (see Table 1 and facies association discussions below), and facies group 2 as lower flow regime (LFR) and normal deposition rates to HDR deposits (see Table 2 and facies association discussions below).

Mudrock facies group 1 (Fig. 5; Table 3) consists of mudrock that is gray, gray-green, brown, or black in color. This facies group composes approximately 64% of the mudrock facies in the three measured sections combined and includes globular gray mudrock (M1.1–3%), black mudrock (M1.2–3%), brown to dark gray mudrock (M1.3–18%), gray-green mudrock (M1.4–4%), and gray mudrock (M1.5–37%). Mudrock facies group 2 (Fig. 6; Table 4) consists of mudrock that is dominantly purple, red, or variegated in color. This facies group composes approximately 36% of the mudrock facies of this dataset and includes purple mudrock (M2.1–18%), red mudrock (M2.2–16%), and mudrock with variegated color (M2.3–2%).

Some sandstones of Facies S1.6 also occur as tabular deposits 0.20–3 m thick interbedded with mudrock facies as documented below in facies associations 4–6 (Fig. 7; Table 5). Some mudrocks also occur in amalgamated and lenticular lithosomes as documented in facies associations 2 and 3 (Figs. 8, 9; Table 5).

Below, we distinguish three sandstone-dominated and three mudrock-dominated facies associations. The sandstone facies associations 1–3 are recognized based on the degree of sandstone amalgamation and the proportion of sandstone and mudrock facies, and mudrock facies associations 4–6 by the proportion of mudrock facies groups 1 and 2.

Facies Association 1 (FA 1): Sandy Channel Lithosomes

Facies association 1 characteristically consists of 10–50-m-thick, erosionally bounded sandstones that have a massive or uniform appearance in outcrop (Fig. 8A), except for > 1-m-thick mud-clast conglomerates that

TABLE 1.—*Sandstone facies group 1: sandstones and conglomerates with planar to low-angle, concave- to convex-up laminae, or devoid of structure.*

Facies	%	Description	Interpretation
S1.1 Conglomerates	14%	Composed dominantly of granule-to boulder-size angular to subrounded mudrock rip-up clasts surrounded by a sandy matrix. Locally, granules of quartzite (dominant) and chert are present. Common at the bases of channel scours and flat erosion surfaces. Most deposits contain randomly oriented clasts and reach thicknesses up to 3 m. Some deposits are stratified and imbricated and found in composite bedsets ranging in thickness from several decimeters to several meters thick.	Locally derived from floodplain deposits resulting from bank undercutting, collapse, and transport under supercritical flow conditions.
S1.2 Sandstones with scour-and-fill structures	21%	Quartzose-to-arkosic, buff to yellow sandstone. Grain sizes range from medium to very coarse with localized lenses of conglomeratic sandstone with gravel-size grains. Subangular to subrounded. Poorly to moderately sorted. Scoured surface at the base, filled with upward-flattening laminae with dip angles ranging from 20° to $< 5°$. Dip directions of laminae are multimodal, even within the same bedsets. Fill styles range from asymetrical to symetrical. Thicknesses range from decimeters to several meters. Widths range from decimeters to 10s of meters.	Supercritical flow, high deposition rates, suspension deposition, large antidune, cyclic steps, or chute-and-pool formation.
S1.3 Sandstones with planar to low-angle laminae	19%	Quartzose-to-arkosic, buff to yellow sandstone. Grain sizes range from fine to very coarse. Subangular to subrounded. Poorly to moderately sorted. Planar to low-angle ($< 10°$) stratification with distinct laminae. Dip directions are mostly to the north and northwest. Thicknesses range from decimeters to a several meters.	Supercritical or transcritical flow, high deposition rates, suspension deposition, plane bed to antidune formation.
S1.4 Sandstones with convex-up long-wavelength laminae	8%	Quartzose-to-arkosic, buff to yellow sandstone. Grain sizes range from medium to coarse. Subangular to subrounded. Poorly to moderately sorted. Very low angle, long-wavelength cross strata with upward-increasing steepness. Dip directions are mostly to the north and northwest. Thicknesses of laminae sets range from decimeters to a few meters. Widths range from meters to 10s of meters.	Supercritical flow, high deposition rates, suspension deposition, antidune formation.
S1.5 Sandstones with soft-sediment deformation	5%	Quartzose-to-arkosic, buff to yellow sandstone. Grain sizes range from Medium to coarse with occasional lenses of gravel-size grains. Subangular to subrounded. Poorly sorted. Soft-sediment-deformed laminae that form anticlinal to domal structures that transition laterally and/or vertically into other facies within group 1. Thicknesses range from 1 m to 10s of meters.	Water escape or local collapse.
S1.6 Structureless sandstones	18%	Quartzose-to-arkosic, buff to yellow sandstone. Grain sizes range from fine to coarse. Subangular to subrounded. Poorly to moderately sorted. Often weakly cemented. No visible sedimentary structures. Thicknesses range from decimeters to 10s of meters.	High deposition rates, suspension deposition. Could also indicate disruption of sedimentary structures by compaction prior to cementation. Weakly cemented deposits may contain structures that are not visible on the surface due to weathering and erosion.

occur above basal erosion surfaces and some internal erosion surfaces (Fig. 10A, D). Vertical amalgamation of these erosionally bounded sandstones results in cliff outcrops that can reach thicknesses of > 100 m in the northern San Juan Basin. Where measured, individual erosionally bounded lenses range from 172 to 1564 m in width. The extensive lateral amalgamation of the individual lenses with crosscutting basal scours gives the sandy lithosomes a tabular appearance (Fig. 8A). Low-angle ($< 10°$) downstream- or upstream-dipping accretion sets are observed in outcrops that are oriented approximately parallel to the prevailing flow direction (north to south) (Fig. 10B). Accretion sets consist of amalgamated sandstones or are in places separated by mud-clast conglomerates (Fig. 10A). UFR and HDR sedimentary structures are dominant as sandstone facies group 1 forms 96% (Fig. 9A). Commonly, the UFR structures transition into other styles of UFR structures laterally and vertically (Fig. 10C). For example, a commonly encountered facies succession in the Cuba Mesa Member starts with a basal erosion surface overlain by a thick mud-clast conglomerate (Facies S1.1), which is then overlain by vertical alternations of scour-and-fill (S1.2) and planar to low-angle laminae (S1.3) (Fig. 9A). In some examples, the scour-and-fill structures truncate the underlying planar to low-angle laminae. In other examples, the transitions are the result of upward steepening or, in contrast, flattening of the laminae. It is also common to see thick and laterally extensive deposits with stacked scour-and-fill structures (Fig. 9A). Some deposits are bioturbated from the top down or from accretion set boundaries with vertical burrows that are commonly > 1 m in length (Fig. 10E).

Facies Association 1 Interpretation.—The dominance of UFR sedimentary structures in erosionally based amalgamated sandstones (sandstone facies group 1) indicates dominant deposition under Froude supercritical flow regime and is a key characteristic of variable-discharge rivers (see reviews in Fielding 2006; Fielding et al. 2009, 2018; Plink-Björklund 2015, 2019).

TABLE 2.—*Sandstone facies group 2: sandstones with steeply dipping cross strata and laminae.*

Facies	%	Textures	Interpretation
S2.1 Cross-stratified sandstones	11%	Quartzose-to-arkosic, buff to yellow sandstone with high-angle (≈ 30°) planar and trough cross strata. Grain sizes range from medium- to lower-coarse. Subrounded. Moderately to poorly sorted. Recognized by cross-sets with consistent foresets that display no change in dip angle. Dip directions are to the south and southeast. Thicknesses of cross-sets range from decimeters to ≈ 1 m. Thicknesses of bedsets range from several decimeters to several meters.	Subcritical flow, normal deposition rates, bedload deposition, formed by the migration of dunes.
S2.2 Sandstones with climbing cross strata	0.1%	Quartzose-to-arkosic, buff to yellow sandstone with high-angle (≈ 30°), climbing cross-stratification. Grain sizes range from medium- to lower-coarse. Subangular to subrounded. Moderately to poorly sorted. Recognized by high-angle (≈ 30°) foreset laminae with inclined set boundaries, dipping to the north and opposite to the south dipping cross strata. Thickness of cross-sets range from a few centimeters to approximately several decimeters. Thicknesses of bedsets range from decimeters to ≈ 2 m.	Subcritical flow, high deposition rates, suspension and bedload deposition, formed by the migration and aggradation of dunes.
S2.3 Sandstones with scours and climbing cross laminae	2%	Quartzose-to-arkosic, buff to yellow sandstone. Grain sizes range from upper fine to medium. Subangular to subrounded. Moderately to poorly sorted. Scoured surface at the base, filled with ripple laminae with inclined set boundaries. The angle of ripple-lamination boundaries are upward flattening. Thicknesses of cross-sets are < 3 cm. Thicknesses of bedsets range from a few centimeters to a few meters.	Supercritical to subcritical flow, high deposition rates, suspension and bedload deposition.
S2.4 Sandstone with overturned cross strata or laminae	2%	Quartzose-to-arkosic, buff to yellow sandstone. Grain sizes range from medium- to lower-coarse. Subangular to subrounded. Moderately to poorly sorted. Recognized by clear set boundaries that are deformed and contain oversteepened foreset laminae (> 30°) that dip to the south. Thicknesses of cross-sets range from several centimeters to several decimeters. Thicknesses of bedsets range from ≈ 1 to a few meters.	Deposition under subcritical flow conditions. Subsequent deformation likely occurred under supercritical flow conditions. Paleoflow direction is in the direction of overturning.

TABLE 3.—*Mudrock facies group 1: gray-brown-black mudrock.*

Facies	%	Description	Interpretation
M1.1 Globular mudrock	3%	Dominantly gray to dark-gray mudrock with large, concave-up, globular soft-sediment-deformation features. Grain sizes range from clay to silt. Thicknesses range from 1 to a few meters.	Deformation of floodplain muds due to loading as sediment is deposited in the overlying channel.
M1.2 Black mudrock	3%	Very dark gray to black mudrock with moderate subangular, blocky peds. Grain sizes range from clay to silt. High organic content. Slickensides common.	Floodplain deposition. Reducing to poorly drained soil conditions. Black indicates presence of organic matter or manganese oxide minerals.
M1.3 Brown to dark gray mudrock	18%	Brown to dark gray mudrock, often with relect lamination and plant fragments. Grain sizes range from clay to silt.	Floodplain deposition. Reducing to poorly drained soil conditions. Laminae and preserved organic matter indicate a lack of pedogenesis. Soils were likely buried before pedogenesis could take place.
M1.4 gray-green mudrock	4%	gray mudrock with extensive green mottling and weak to moderate blocky peds. Grain sizes range from clay to silt. Rare slickensides.	Floodplain deposition. Reducing to poorly drained soil conditions. Green mottling indicates localized reduction of ferric minerals or removal of organic matter and oxides due to water saturation and anoxia.
M1.5 gray mudrock	37%	Dominantly gray mudrock. Grain sizes range from clay to silt. Structureless or with angular blocky peds. Devoid of mottling or containing minor green, purple, and/or red mottling. Some structureless deposits contain small lignitized plant fragments and visible quartz granules.	Floodplain deposition. Reducing to poorly drained soil conditions or lack of pedogenic development.

TABLE 4.—*Mudrock facies group 2: purple-red mudrock.*

Facies Name	Facies %	Textures	Interpretation
M2.1 Purple mudrock	18%	Dominantly purple mudrock with weak to moderate blocky peds. Yellow-brown mottles are common. Rarely, gray-green mottles are also present. Grain sizes range from clay to silt. Some deposits contain slickensides	Floodplain deposition. Weak hematite impregnation. Moderately poorly drained soil conditions. Pedogenic modification. Gray and yellow-brown mottles and slickensides are the result of soil gleying, and indicate that the soils were episodically saturated.
M2.2 Red mudrock	16%	Dominantly red (pink to maroon) mudrock with moderate to strong blocky peds. gray mottles are common. Slickensides are common. Grain sizes range from clay to silt. Some horizons contain large (> mm) carbonate nodules.	Floodplain deposition. Moderately to well-drained and oxidizing soil conditions. Pedogenic modification. gray mottles are likely root traces. Presence of carbonate nodules indicate well-drained and oxidizing conditions. Slickensides are the result of soil gleying and indicate that the soils were episodically saturated.
M2.3 Mudrock with variegated color	2%	Mudrock with abundant, varicolored mottling of gray-green, yellow-brown, purple, and red and strong wedge-shaped peds. Slickensides are abundant. Grain sizes range from clay to silt.	Floodplain deposition. Episodic soil saturation. Extensive pedogenic development.

Comparison of the documented UFR facies to experimentally produced deposits (Alexander et al. 2001; Cartigny et al. 2014; Ono et al. 2020) indicates deposition by migration of antidunes as well as cyclic steps (Table 1). Antidune migration produces upstream- or downstream-dipping low-angle lamination that commonly display convex-up shapes with planar laminae forming between the antidunes (Alexander et al. 2001; Cartigny et al. 2014), such as in facies S1.3 and S1.4 (Table 1, Fig. 2). Low-angle bedforms can also form by the flattening of dunes at the transition to upper-stage plane beds (e.g., Naqshband et al. 2017), but the presence of upstream-dipping laminae (backsets) suggests that the supercritical-flow origin is more likely, as dunes can migrate only downstream. Furthermore, the upward-flattening to upward-steepening trends are a characteristic of antidunes and form as scours are filled and antidune mounds aggrade, respectively (West et al. 2019). The nearly planar, subhorizontal geometry (S1.3) formed in experiments at lower aggradation rates and bedform amplitude increased with higher aggradation rates, producing backsets or foresets and convex-up laminae (S1.4) (Cartigny et al. 2014). The documented scour-and-fill and consistent backset deposits (S1.2) are similar to experimentally produced deposits from migrating cyclic steps (Cartigny et al. 2014; Ono et al. 2020). In contrast to fully supercritical flow that produces antidunes in cyclic steps, the flow abruptly shifts to subcritical at hydraulic jumps and then accelerates to supercritical again downstream. Erosion occurs in the steep supercritical zone upstream of the hydraulic jump and deposition occurs at the hydraulic-jump scour, producing scour-and-fill structures. Backsets form at the downstream edge of the scour as the cyclic steps migrate upstream (e.g., Cartigny et al. 2014; Ono et al. 2020). Ono et al. (2020) show that cyclic steps alone can produce complex lamination that include scour-and-fill structures and planar to low-angle laminae with foresets and backsets. Scour-and-fill and consistent backsets form at hydraulic jumps and lower-angle laminae form farther downstream, such as is observed in some outcrops (Fig. 3A). In these experiments, consistent backsets formed only when the migration of the hydraulic jumps was stable (Ono et al. 2020). Regardless of the specific bedform regime responsible for the creation of these structures, facies S1.2, S1.3, and S1.4 are indicative of deposition under Froude supercritical flow conditions. The experiments further show a dominance of suspension transport of sands (Alexander et al. 2001; Cartigny et al. 2014; Ono et al. 2020), and even gravels (Ono et al. 2020), at high deposition rates under supercritical flow. This abundance of suspension transport and rapid deposition is corroborated by the aggradational nature of the sedimentary structures and the gradational or diffuse laminae (Fig. 2) (see Duller et al. 2010). High deposition rates are likely to be essential for accumulating large thicknesses of UFR deposits that otherwise have a very low preservation potential (Allen and Leeder 1980; Cheel 1986; Bridge and Best 1988, 1997; Paola et al. 1989; Alexander et al. 2001). In places, soft-sediment deformation (S1.5) and structureless sandstones (S1.6) occur in association with the UFR sedimentary structures, especially in large hydraulic-jump scours (Fig. 3B). Structureless deposits were commonly produced at hydraulic jumps in experiments due to the abrupt loss of capacity where flow transitions from supercritical to subcritical (Alexander et al. 2001; Cartigny et al. 2014). Soft-sediment deformation formed by porewater escape due to rapid deposition, as well as by partial gravitational collapse from steep hydraulic jump scour margins towards the scour base (Cartigny et al. 2014; Ono et al. 2020).

Supercritical flow conditions occur in many rivers during seasonal floods, such as those that occur in monsoon zone rivers (e.g., Kale et al. 1994), or floods with up to multidecadal occurrence, such as those that occur in subhumid or arid rivers (Alexander et al. 1999a; Amos et al. 2004). A general lack of transitions from UFR structures to ripples or dunes implies extremely rapid decline in flood flow velocity (Jones 1977) or complete reworking during consecutive floods (Amos et al. 2004). Evidence for high deposition rates and suspension transport of sand- to granule-size sediment further indicates deposition by seasonal rivers which are likely to have high sediment yields compared to rivers from perennial precipitation zones (Cecil et al. 2003). The suspended load in some modern subtropical rivers has been suggested to be about 20 times higher than in persistent-discharge rivers (Frostick and Reid 1977). The high percentage of UFR structures observed in this lithosome is similar to some of the deposits of the most extreme modern variable-discharge river systems that receive their total annual precipitation in just a few downpours (Sneh 1983; Stear 1985; Billi 2007) and have been shown to consist of 80–100% UFR sedimentary structures (Plink-Björklund 2015). Similar channel lithosome styles have been hypothesized to consist entirely of high-magnitude flood deposits (Plink-Björklund 2015; Wang and Plink-Björklund 2020) because they share many characteristics with flash-flood deposits (Schumm 1961; McKee et al. 1967; Williams 1971; Stear 1985; Billi 2007).

The thick mud-clast conglomerates (S1.1) indicate high floodplain erosion and channel bank collapse or flowage rates (Karcz 1969; Laury 1971). Conglomerates with randomly oriented, angular to subangular, matrix-supported clasts indicate minimal current reworking and are likely to be derived from bank failure. Riverbanks are undercut during floods, and develop shear cracks, whereby parts of the bank slump during the falling stage of floods (Coleman 1969; Gohain and Parkash 1990; Singh et al. 1993). This bank undercutting and successive collapse is linked to high water power and rapid lowering of water level during the waning stage of floods (e.g., Manley et al. 1987; Gohain and Parkash 1990; North and Taylor 1996; Tandon and Gibling 1997). Flowage of bank material into

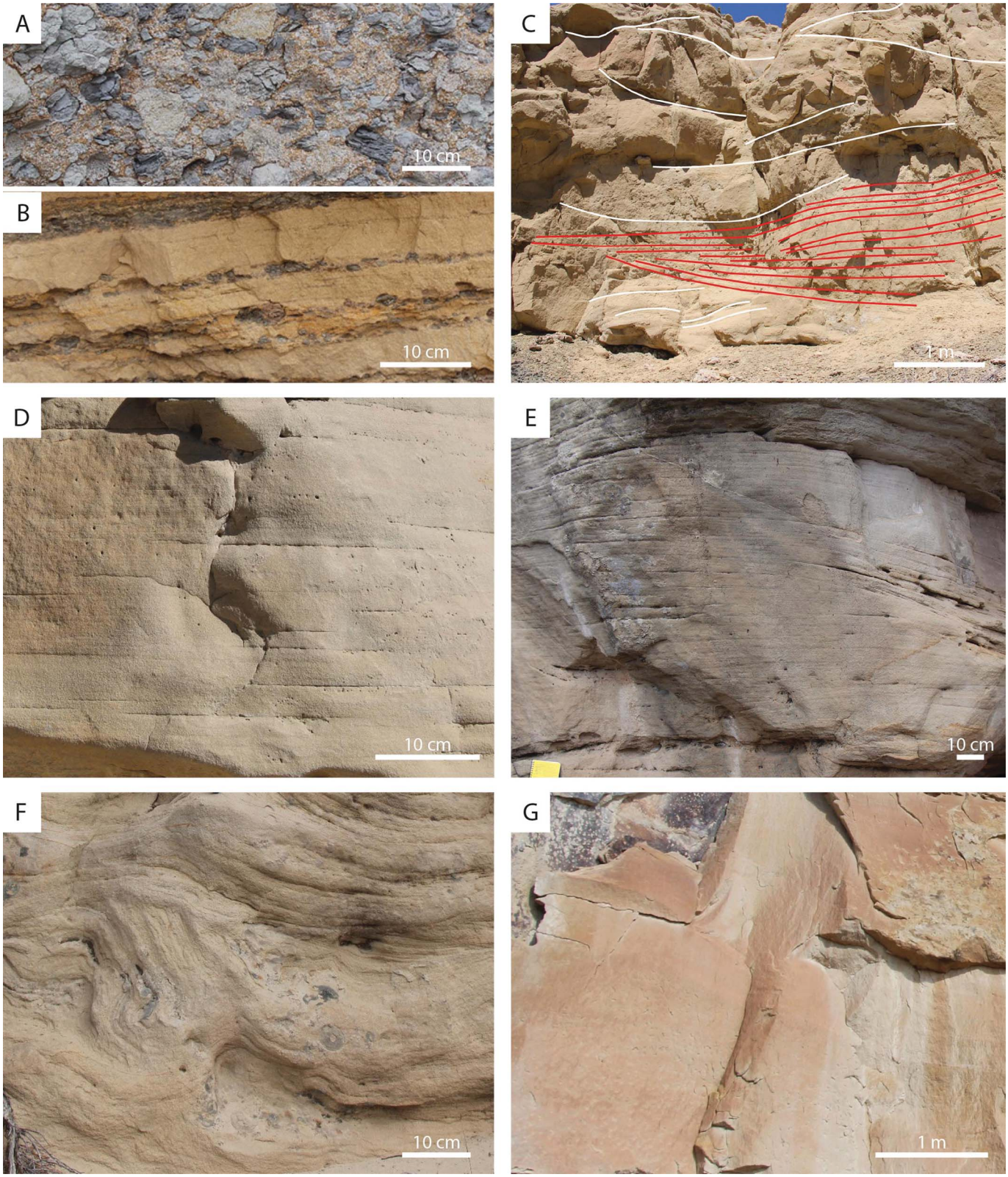

FIG. 2.—Examples of sandstone facies group 1. **A)** S1.1: conglomerate with randomly oriented clasts. **B)** S1.1: conglomerate with stratified and imbricated clasts. **C)** S1.2: sandstone with scour-and-fill structures (annotated). **D)** S1.3: sandstone with planar to low-angle laminae. **E)** S1.4: sandstone with convex-up long-wavelength laminae. **F)** S1.5: sandstone with soft-sediment deformation. **G)** S1.6: structureless sandstone in well-cemented outcrop. **H)** S1.6: seemingly structureless sandstone in poorly cemented outcrops (marked with white arrows) encased in mudrock deposits.

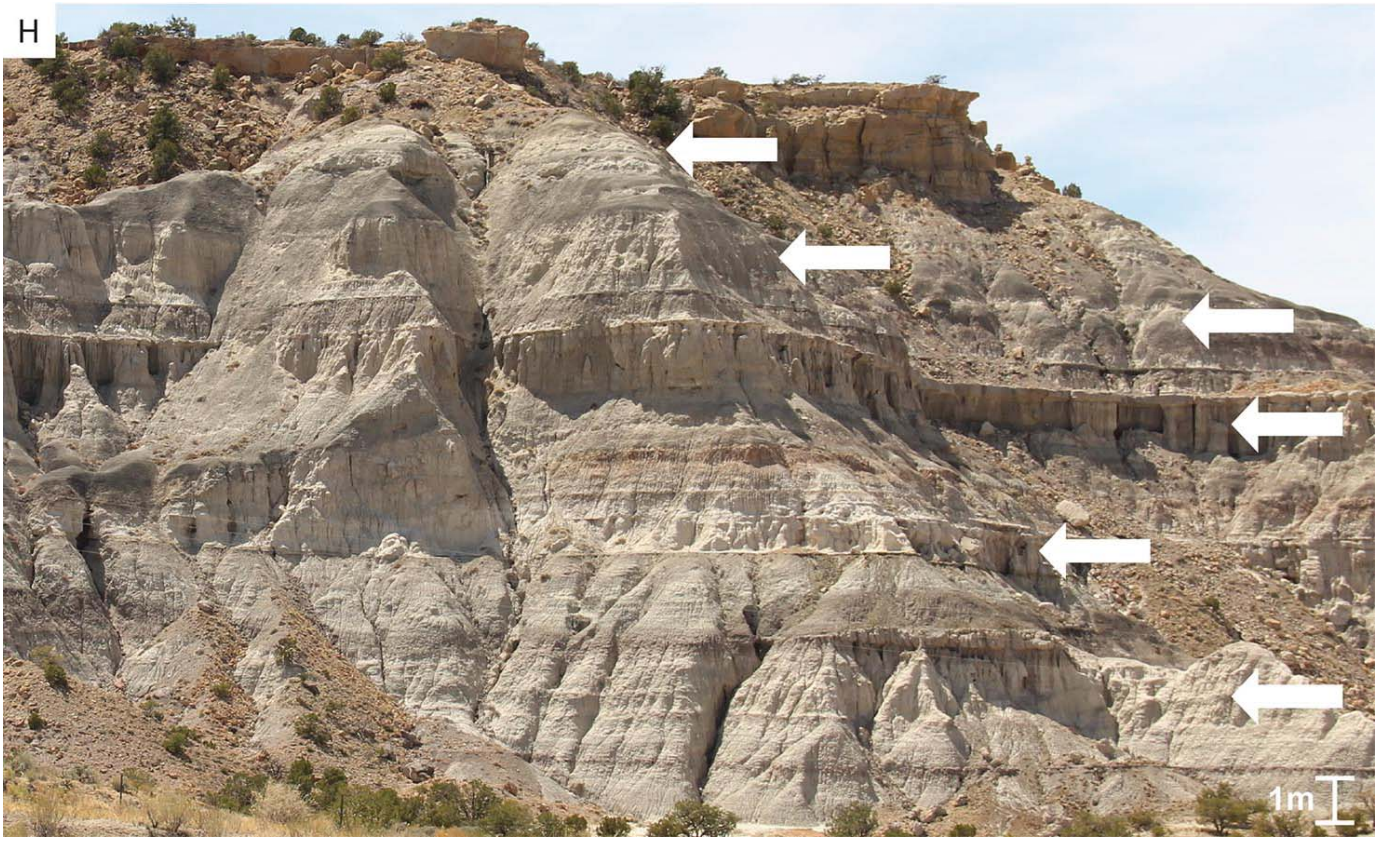

FIG. 2.—Continued.

channels is another failure mechanism that develops when the water level falls rapidly and porewater in the channel banks develops overpressure and failure (Coleman 1969). Such thick conglomerates have also been described from other ancient river deposits (e.g., Deluca and Eriksson 1989; North and Taylor 1996; Plink-Björklund et al. 2014), and are suggested to be common in rivers with variable discharge that experience high-magnitude floods with high water power, high tractive force, and rapid changes in water level (North and Taylor 1996; Plink-Björklund 2015). The stratified and imbricated conglomerates indicate current reworking and transport (Karcz 1969), as also corroborated by the lower degree of clast angularity than is observed in the conglomerates with randomly oriented clasts.

In-channel bioturbation indicates that the channels only transmitted discharge during floods and were seasonally dry or had low perennial base flow (Hasiotis et al. 2007).

In summary, facies association 1 lithosomes appear to consist entirely of high-magnitude flood deposits or flood event beds (e.g., Fig. 10A), because they essentially lack dune or ripple strata. At macroform scale they either display upstream or downstream accretion, where accretion sets are composed of flood event beds and lack indicators of point-bar accretion (lateral accretion, upward fining; e.g., Willis 1993; Bridge et al. 1995) or braid-bar accretion (sets of cross strata at different scales; e.g., Bridge 2003; Lunt et al. 2004). The high degree of channel amalgamation together with a lack of systematic lateral migration (lateral accretion) signifies high avulsion rates (Bryant et al. 1995).

Facies Association 2 (FA 2): Heterolithic Channel Lithosomes

Facies association 2 also consists of abundant sandstones, but these lithosomes contain mudrock layers along accretion set boundaries and flood-event bed boundaries (Fig. 11). As a result, these lithosomes appear less laterally and vertically amalgamated in outcrop than those of FA 1 (Figs. 8B, 9B). FA 2 lithosome thicknesses range from 5 to 13 m and widths from 94 to 312 m. Accretion sets dip at a low angle ($< 10°$) in the downstream direction or at a high angle (up to 20°) in the upstream direction in outcrops that are oriented parallel to flow direction (north to south) (Figs. 8B, 11A). The steep upstream accretion sets are erosionally bound and characteristically display basal scours (Figs. 8B, 11A). As a result, each of the strata in the accretion sets has a lenticular shape with erosional upper and lower boundaries (Fig. 8B). UFR and HDR sedimentary structures are still dominant with sandstone facies group 1 at 89%, but there is a larger proportion of lower-flow-regime (LFR) structures of sandstone facies group 2 (11%) compared to FA 1 (Fig. 9B). The most common LFR structures are cross-stratified sandstone (S2.1, 10%) and scours filled with climbing ripple laminae (S2.3, 2%) (Figs. 3, 9B). Lateral variations in facies within individual lithosomes are common. A characteristic facies succession in the upstream-accretion sets is structureless (S1.5) and soft-sediment deformed (S1.6) sandstones, or scour-and-fill sandstones near the basal scours, and an upward and downstream transition into more laminated facies, including planar to low-angle laminae (S1.4), but also cross strata (S2.1) and climbing cross strata (S2.2).

Some deposits are bioturbated from the top down or from accretion set boundaries. Burrows associated with this lithosome are shallower, branching trace fossils (Fig. 11B). Mudrock layers of several decimeters in thickness (Fig. 11A) are gray (M1.3 and M1.5) to purple (M2.1) and commonly display pedogenic modification in the form of mottling and ped structure (Figs. 5, 6, Tables 3, 4). Some of the dark-gray (M1.3) mudrock layers contain plant fragments.

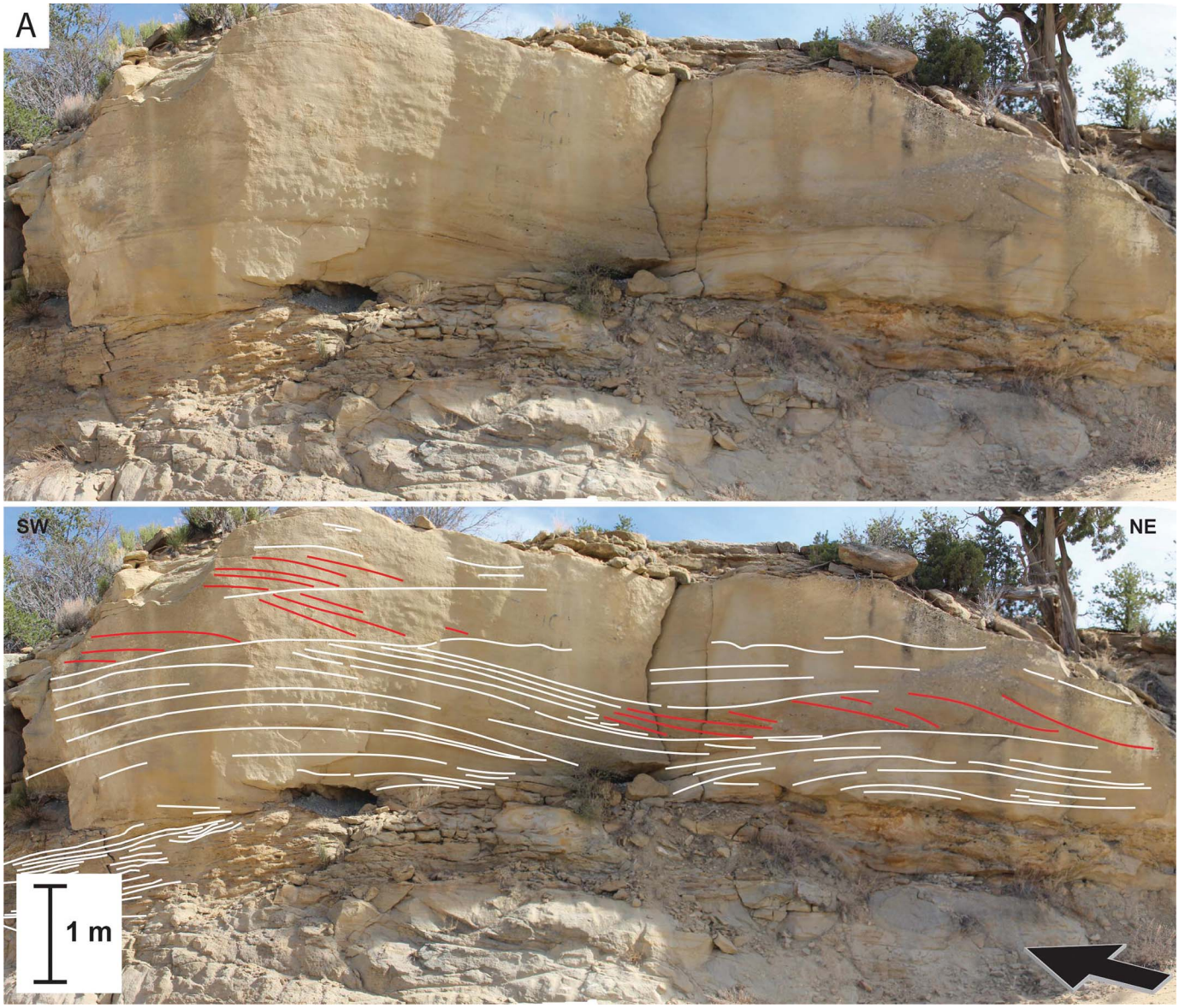

FIG. 3.—Outcrop examples of sandstone facies group 1. **A)** Backsets (annotated in red) with dip directions approximately opposite the prevailing paleocurrent direction (black arrow). The backsets commonly transition downstream into low-angle (S1.3) or convex-up low-angle (S1.4) structures. **B)** Example of an interpreted hydraulic-jump deposit, where abrupt loss of flow capacity at the jump resulted in rapid sediment fallout and a structureless deposit (S1.6) that includes mud clasts. Red arrows show inferred flow directions. Prevailing paleoflow direction is indicated by the black arrow.

Facies Association 2 Interpretation.—The dominance of UFR sedimentary structures in erosionally based amalgamated sandstones (sandstone facies group 1) suggests that most deposition occurred under Froude supercritical flow regime similar to facies association 1, and indicates variable-discharge rivers (see reviews in Fielding 2006; Fielding et al. 2009, 2018; Plink-Björklund 2015, 2019).

In places, the vertical transitions from UFR to LFR structures (e.g., Fig. 9B) may indicate a less-rapid decline in flow strength during the waning phase of floods (Jones 1977). Whereas in upstream-accretion sets, the UFR and LFR structures may have formed at the same time and thus indicate spatial flow fluctuations. Such large-scale erosionally bounded backsets have been recognized in other deposits of variable-discharge rivers and interpreted as channel-scale cyclic-step migration (Wang and Plink-Björklund 2020). Comparison to experimentally produced deposits (Ono et al. 2020) shows coeval deposition of scour-and-fill or structureless strata at the hydraulic jump, and low-angle strata downstream of hydraulic jumps. The highest deposition rates occur at the hydraulic jump, at times resulting in structureless or graded deposits (see also Postma et al. 2009; Postma and Cartigny 2014; Postma 2014). The degree of stratification and lamination increases downstream of the hydraulic-jump scour, where the flow accelerates into transcritical and then again to supercritical conditions (e.g., Cartigny et al. 2014). Dunes and climbing dunes may form in the zone where the flow is still subcritical and deposition rates are lower. Upstream migration of a hydraulic jump may result in a vertical succession where erosional scours are overlain by structureless or soft-sediment-deformed deposits that transition upward into better-stratified deposits (Postma et al. 2009; Postma and Cartigny 2014; Postma 2014; Ono et al. 2020) including cross strata or climbing cross strata (Fig. 9B).

Deposition of in-channel mud horizons has been linked to the waning of high-magnitude floods with a high mud content (Williams 1971; Tunbridge

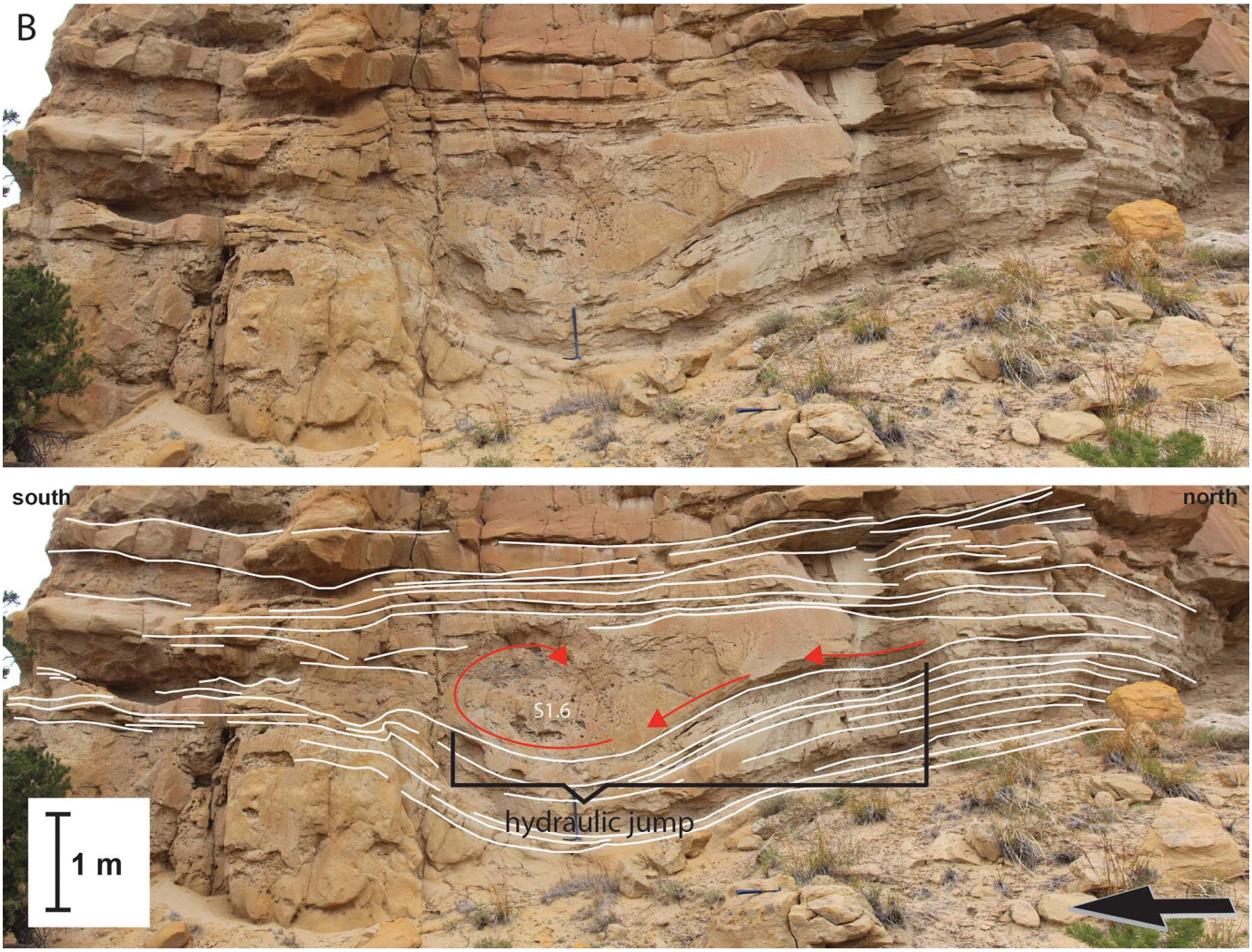

FIG. 3.—Continued.

1981). Newly formed mud drapes at the tops of bars, on accretion surfaces, or at the channel bottom have been observed in modern variable-discharge rivers after major floods (e.g., Stear 1985; Abdullatif 1989; Singh et al. 1993; Billi 2007). For example, after a high-magnitude flood of Kosi River in 1984, a mud layer 30 cm deep, 20 m wide, and 100 m long mud was deposited in a channel (Singh et al. 1993). Experiments show (Ono et al. 2020) that clay and silt can also be deposited at hydraulic jumps without overall flow waning. The presence of bioturbation and pedogenic modification (mottling and peds) indicates that the channels were seasonally or interannually dry or had low perennial base flow (Hasiotis et al. 2007).

In summary, although facies association 2 lithosomes contain a small proportion of LFR structures, some of these structures likely formed coevally with the UFR structures and indicate the inherent spatial variability of the supercritical flow regime. Deposition from sustained supercritical flow is further indicated by consistent large-scale backsets (Fig. 11) that document cyclic-step migration. In addition, facies association 2 lacks indicators of point-bar accretion (lateral accretion, upward fining; e.g., Willis 1993; Bridge et al. 1995) or braid-bar accretion (sets of cross strata at different scales; e.g., Bridge 2003; Lunt et al. 2004), and appears to consist entirely of high-magnitude flood deposits or flood event beds.

Facies Association 3 (FA 3): Lenticular Channel Lithosomes

These lithosomes are isolated and lenticular in shape. The FA 3 thicknesses range from 2 to 17 m and widths from 27 to 282 m. These lenticular deposits range from sandy to heterolithic with mud layers separating sandy accretion sets or sandy strata within the accretion sets (Fig. 12B). In places, the accretion sets occur as channel-scale scour-and-fill structures (Fig. 12A). In some examples, lateral-accretion sets dipping at 10–30° occur where the outcrop exposure is perpendicular to flow. Although still abundant, the content of UFR sedimentary structures is considerably lower, and sandstone facies group 1 forms 50% (Fig. 9C). LFR structures (sandstone facies group 2, 50%) include cross-stratified sandstone (S2.1, 39%), scours filled with climbing-ripple laminae (S2.3, 3%), and overturned cross strata (S2.4, 8%). Vertical and lateral transitions between UFR and LFR structures are frequently observed, although some of the smaller lenticular lithosomes consist entirely of LFR structures (Fig. 12C). Lignitized plant and wood fragments are occasionally found in these lithosomes.

Facies Association 3 Interpretation.—The isolated nature of these lithosomes indicates a lower degree of channel amalgamation. The combination of LFR and UFR sedimentary structures suggests variations

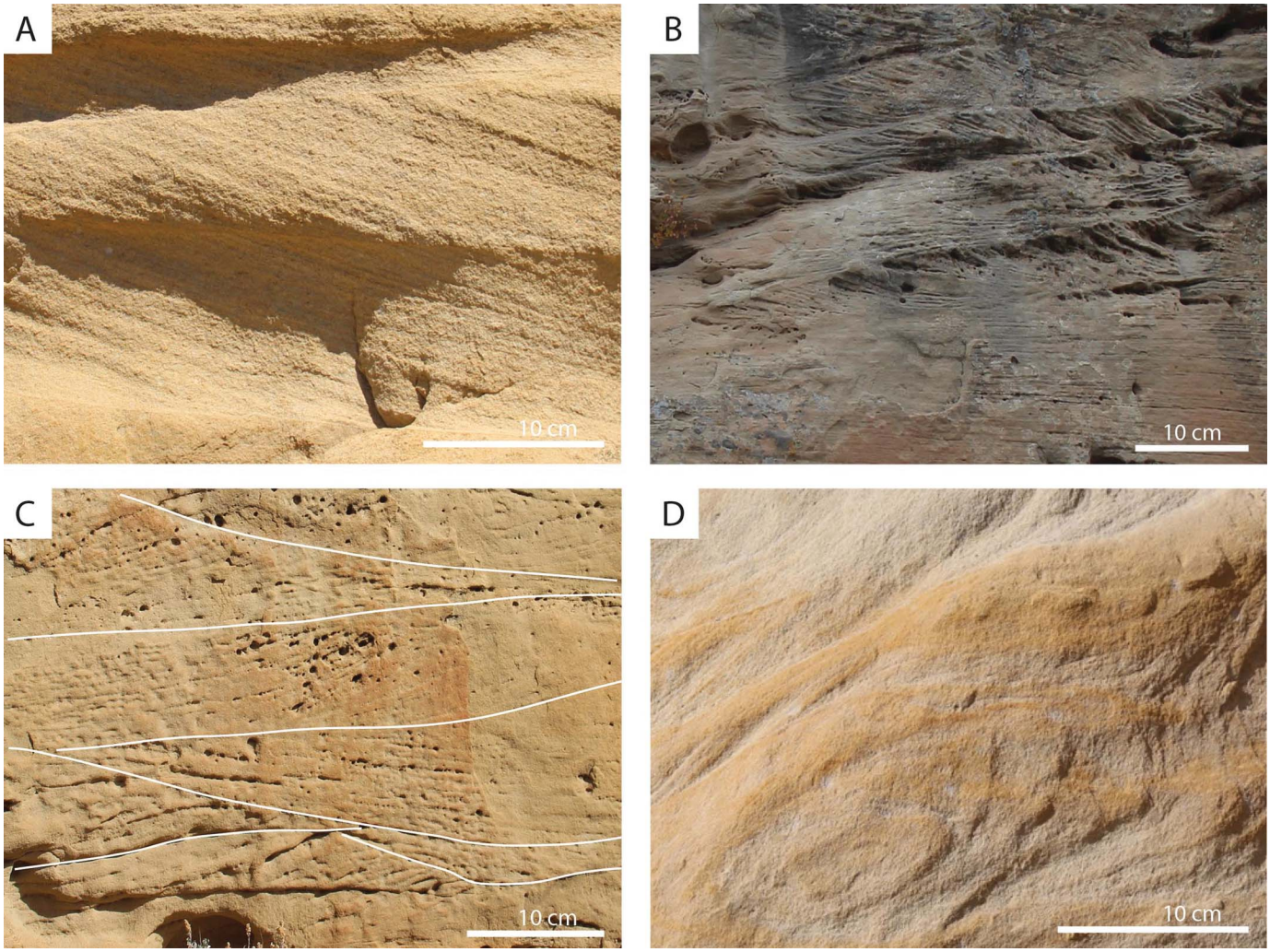

FIG. 4.—Examples of sandstone facies group 2. **A)** S2.1: cross-stratified sandstone. **B)** S2.2: sandstone with climbing cross strata. **C)** S2.3: sandstone with scours and climbing cross laminae. Scour surfaces are annotated in white. **D)** S2.4: sandstone with overturned cross strata or laminae.

between low and high flow velocities, respectively, where rapid deposition in supercritical flow conditions alternated with subaqueous dune migration during more sustained subcritical flow conditions. This presence of cross strata above UFR structures may indicate a less rapid decline of flood strength and preservation of the waning-phase deposits (Abdullatif 1989). Alternatively, the LFR structures may be the result of post-flood reworking of sediment under subcritical flow conditions (Abdullatif 1989). Also, the LFR structures may simply be better preserved due to less erosion during consecutive floods. A modern example of such UFR and LFR deposit variability is the River Gash in Sudan, which experiences high-magnitude floods that last for about a week, but also a wet-season base flow that lasts for the whole monsoon season (Abdullatif 1989).

Channel-scale scour-and-fill architecture (Fig. 12A) suggests conditions controlled by discharge variability and supercritical flow and have been documented in other deposits of variable-discharge rivers (Wang and Plink-Björklund 2020). Lateral-accretion sets, however, indicate sustained bar migration as determined by subcritical flow conditions.

In summary, facies association 3 preserves approximately equal proportions of LFR and UFR structures, and on macroform scale contains both lateral-accretion sets characteristic for subcritical flow and channel-scale scour-and-fill geometries formed in supercritical flow.

Facies Association 4 (FA 4): Poorly Drained Floodplain Lithosomes

Facies association 4 consists of vertically stacked deposits of dominantly mudrock facies group 1 (gray-brown-black mudrock, 95%), including globular gray mudrock (M1.1), black mudrock (M1.2), brown to dark gray mudrock (M1.3), gray-green mudrock (M1.4), and gray mudrock (M1.5). Deposits of mudrock facies group 2 are rarely observed in this facies association (purple-red mudrock, 3%). Most of the mudrock layers are tabular, but there are also occasional scour surfaces filled with brown to dark gray mudrock (M1.3) (Fig. 7A). Vertical successions show alternations of mudrocks lacking visible evidence of pedogenic modification and commonly exhibiting preserved organic matter and/or relict lamination (M1.3 and some deposits of M1.5) with more strongly developed paleosols displaying soil structure (peds) and/or mottling (M1.2, M1.4, and deposits of M1.5 with weak to moderate angular blocky peds). Thin, tabular or lenticular, and poorly cemented buff-colored sandstones (S1.6, 2%) are commonly interbedded in the mudrock succession (Fig. 7A) and range in thickness from 0.20 to 3 m. These sandy deposits are difficult to distinguish from the surrounding mudrock facies because all of them display a similar style of badland erosion, forming steep slopes ($> 45°$) that are commonly capped with well-cemented, cliff-forming channel

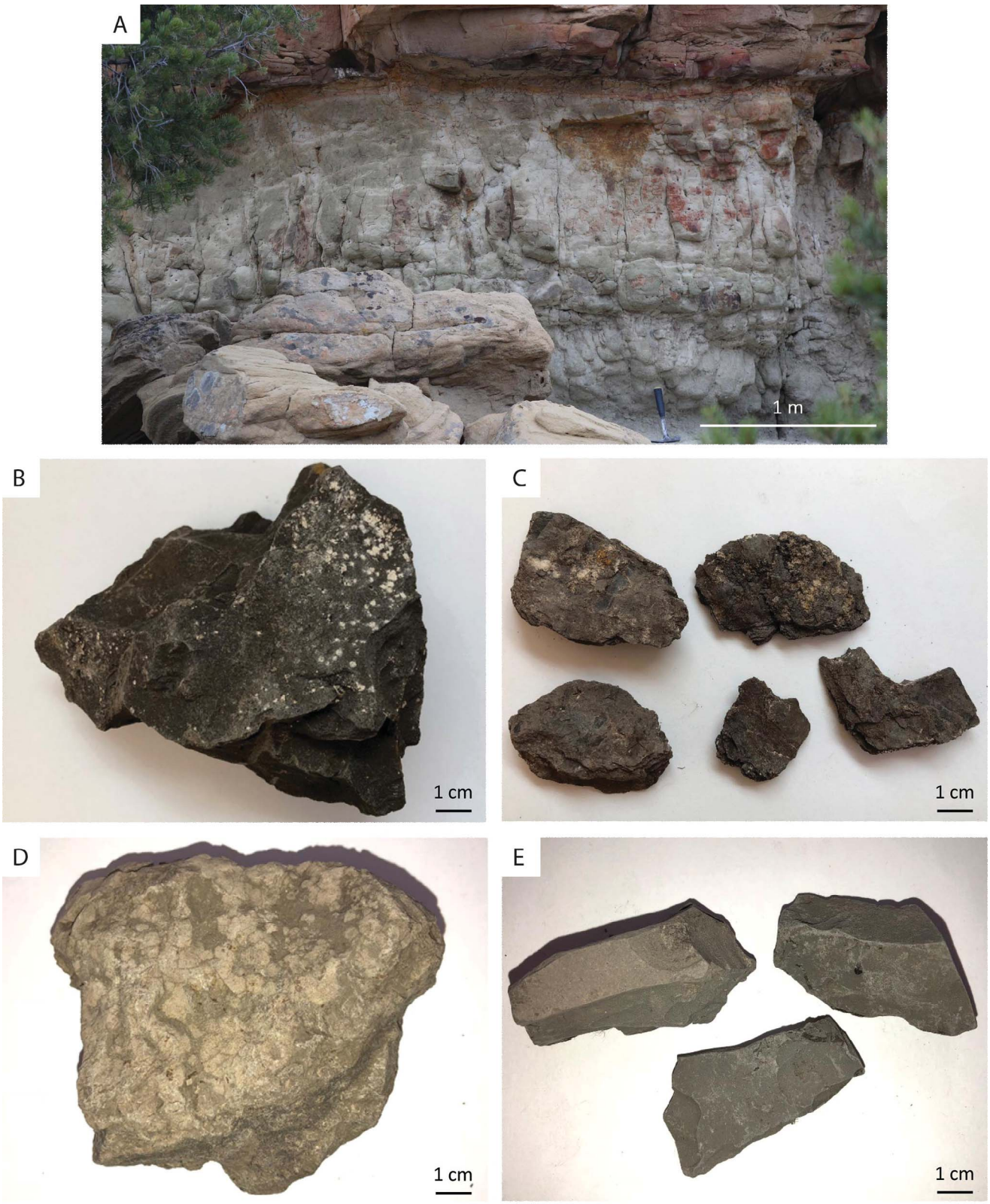

FIG. 5.—Example hand samples of mudrock facies group 1. **A)** M1.1: globular gray mudrock. **B)** M1.2: black mudrock. **C)** M1.3: brown to dark gray mudrock with relict lamination and plant fragments. **D)** M1.4: gray-green mudrock. **E)** M1.5: gray mudrock.

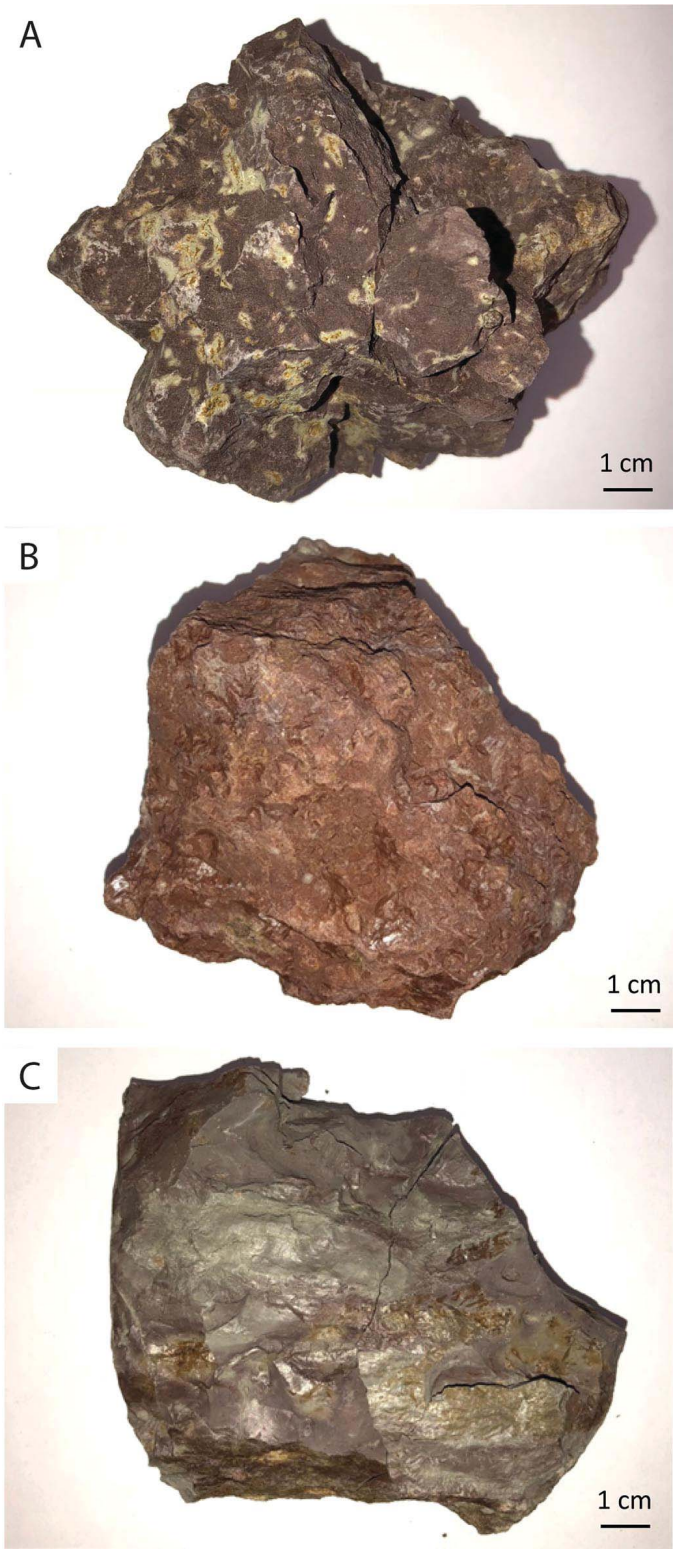

FIG. 6.—Example hand samples of mudrock facies group 2. **A)** M2.1: purple mudrock with yellow-brown mottles. **B)** M2.2: red mudrock. **C)** M2.3: mudrock with variegated color.

deposits (Fig. 7A) and a thick interval (> 1 m) of globular gray mudrock (M1.1) at the bases of the channels.

Facies Association 4 Interpretation.—Mudrock deposits with black (Facies M1.2) or dark brown colors (Facies M1.3) are commonly attributable to the presence of organic matter or manganese oxide minerals (Farnham and Kraus 2002; Vepraskas 2016; Tabor et al. 2017). Gleyed colors including gray and green (Facies M1.4 and M1.5) are thought to be the result of reduction of ferric minerals or removal of organic matter and oxides, which are processes associated with water saturation and anoxia (Farnham and Kraus 2002; Vepraskas 2016; Tabor et al. 2017). The poorly cemented buff sandy deposits are likely crevasse splays where thin and tabular, and isolated channel deposits where lenticular. The crevasse-splay deposits indicate partial avulsions, which causes channels to shift their positions on the floodplain (Bridge and Leeder 1979; Jones and Schumm 1999). This process can end sedimentation to part of the floodplain for a period of time, leading to pedogenic development of surface deposits (Kraus 1999). Meanwhile, the location occupied by the overbank flow of the partial avulsion experiences a high rate of sedimentation that prevents pedogenic development (Kraus 1999). The large, globular soft-sediment-deformation structures (Facies M1.1) likely resulted from loading of wet floodplain muds by sand deposited above, similar to ball-and-pillow structures (Mills 1983).

The facies in the FA 4 lithosome display a range of pedogenic development levels, from mudrocks lacking visible pedogenic modification to more strongly developed paleosols. Similar styles of stacked mudrock deposits are interpreted to record variations in the balance between sediment accumulation and the rate of pedogenesis (Marriott and Wright 1993; Kraus 1999). Pedogenic development can occur only on land surfaces that are relatively stable for a period of time (Ruhe 1956; Marriott and Wright 1993), and vertically stacked paleosols are formed in sedimentary systems undergoing net aggradation, where the rate of sedimentation does not overwhelm the rate of pedogenesis (Kraus 1999). The vertically stacked profiles containing both mudrocks lacking visible pedogenic development and weakly to moderately developed paleosols indicate that sedimentation was rapid and unsteady at times, precluding the development of strongly developed soils (*sensu* compound to composite paleosols of Kraus 1999). Some scoured surfaces in the floodplain successions indicate that some soil profiles may have been truncated due to erosion of the upper part of a developing soil (Marriott and Wright 1993; Kraus 1999). The stacked floodplain deposits overlying the scour surface indicate that episodes of erosion and truncation were eventually followed by renewed sedimentation (*sensu* Marriott and Wright 1993). The combination of compound to composite paleosols and erosion surfaces is thought to result from an unstable floodplain (Marriott and Wright 1993; Kraus 1999). The presence of relict planar lamination (some deposits of M1.3) filling some scoured surfaces may indicate the presence of standing water (ponding) on parts of the floodplain. Taken together, the combination of facies in this association indicates periods of net aggradation through high deposition rates alternating with times of landscape stability or erosion in a frequently wet depositional environment.

Facies Association 5 (FA 5): Variably Drained Floodplain Lithosomes

Facies association 5 consists of vertically stacked deposits of both mudrock facies group 1 (gray-brown-black mudrock, 46%) and mudrock facies group 2 (purple-red mudrock, 22%), with interbedded thin, tabular, and poorly cemented sandstone deposits (S1.6, 32%) (Fig. 7B). Similar to FA 4, these vertical successions show alternations of mudrock deposits lacking visible pedogenic modification (M1.3 and some deposits of M1.5) and paleosols. However, the paleosols in this facies association contain moderately to strongly developed peds and abundant slickensides, and display a range of colors including gray-green (M1.4), purple (M2.1), red

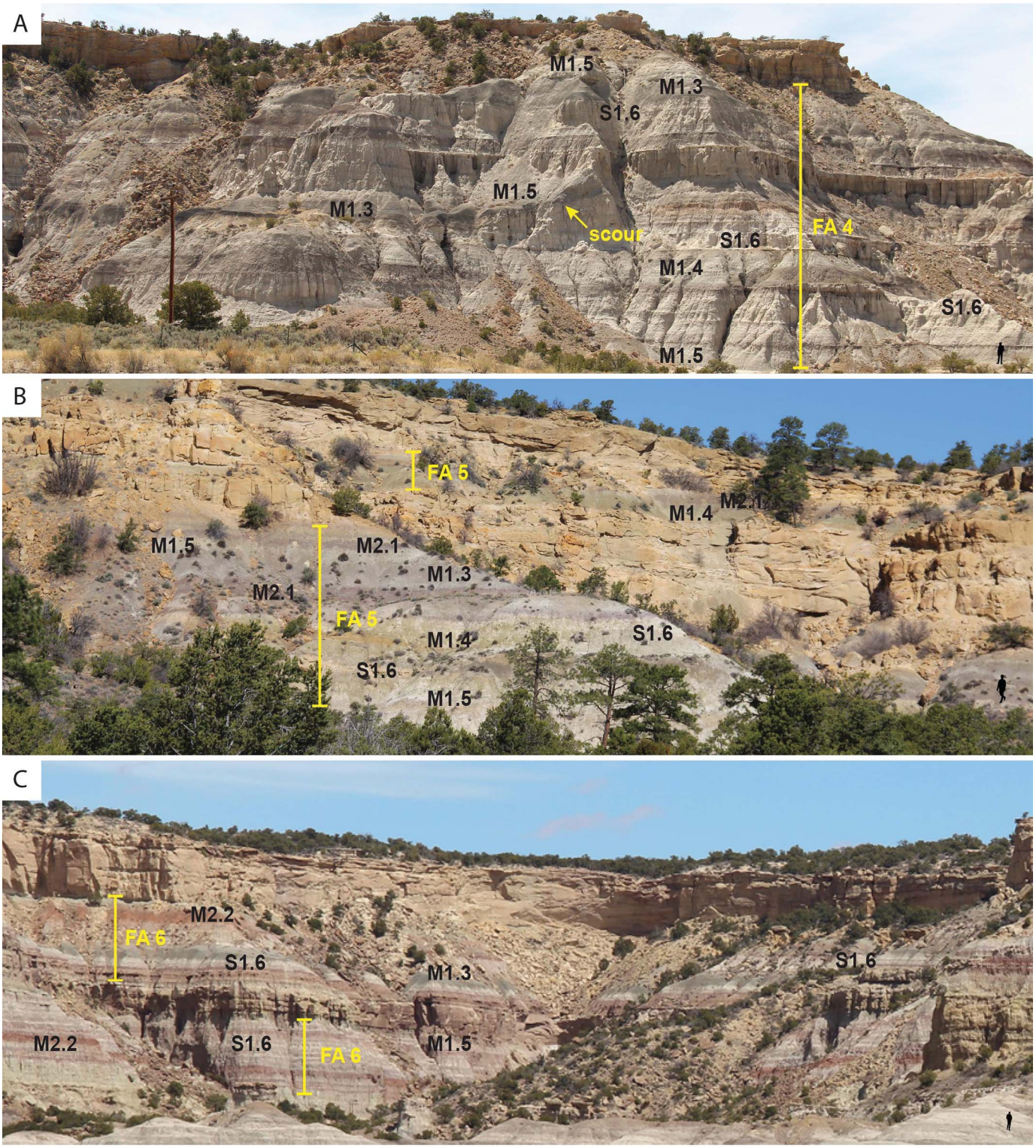

FIG. 7.—Examples of floodplain lithosomes. Several representative horizons are annotated with their corresponding facies abbreviation. Human scale (black silhouette in lower-right corners) is 1.8 m in height. **A)** Poorly drained floodplain lithosomes (FA 4) are dominated by gray-brown-black mudrock deposits (mudrock facies group 1) and interbedded thin crevasse-splay deposits (S1.6). The arrow points to a scour surface that truncates a succession of floodplain deposits and is subsequently filled with a series of stacked floodplain deposits. **B)** Variably drained floodplain lithosomes (FA 5) consist of both gray-brown-black mudrock (mudrock facies group 1) and purple-red mudrock (mudrock facies group 2), interbedded with occasional crevasse-splay deposits (S1.6). **C)** Well-drained floodplain lithosomes (FA 6) consist of abundant purple-red mudrock (mudrock facies group 2), alternating with some gray-brown-black mudrock (mudrock facies group 1) and thin crevasse-splay deposits (S1.6).

TABLE 5.—*Channel and floodplain facies associations.*

Facies Association Name	Included Facies	Description	Interpretation
FA 1 Sandy Channel Lithosomes	S1.1; S1.2; S1.3; S1.4; S1.5; S1.6; S2.1; S2.5	Channel deposits composed of stacked, thick (10-50 m), and erosionally bounded flood units with a massive or uniform appearance in outcrop. Soft-clast coglomerates are often present at the bases of flood units. Dominance of UFR and HDR sedimentary structures (96% Sandstone Facies Group 1). Bioturbation is common at the tops of the flood units.	High-magnitude flood deposits from flash-flood events. Bioturbation indicates that the channel was dry between flooding events.
FA 2 Heterolithic Channel Lithosomes	S1.1; S1.2; S1.3; S1.4; S1.5; S1.6; S2.1; S2.3; M1.3; M1.5; M2.1	Channel deposits composed of stacked flood units and mud layers along accretion-set boundaries. UFR and HDR sedimentary structures are abundant (89% Sandstone Facies Group 1), with a larger proportion of LFR structures (Sandstone Facies Group 2: 11%) than FA 1 channels.	High-magnitude-flood deposits with preservation of waning flow stage, possibly indicating a less rapid decline in flow strength than the FA 1 channels. Where present, in-channel pedogenic development of mudrock indicates that the channel was dry between flooding events, allowing soil development.
FA 3 Lenticular Channel Lithosomes	S1.2; S1.3; S1.4; S1.5; S1.6; S2.1; S2.3; S2.4; M1.3; M1.5; M1.2	Isolated channel deposits that are lenticular in shape and bounded by floodplain deposits. Channel fill ranges from sandy to heterolithic. Lesser abundance of UFR and HDR sedimentary structures (50% Sandstone Facies Group 1) and higher abundance of LFR structures (50% Sandstone Facies Group 2).	Channels transported lesser discharge and have a lower degree of amalgamation than the highly amalgamated FA 1 and FA 2 channels. Combination of LFR and UFR sedimentary structures indicates variations between high and low flow velocities and less-rapid decline of flood strength.
FA 4 Poorly drained Floodplain Lithosomes	M1.1; M1.2; M1.3; M1.4; M1.5; M2.1; S1.6	Vertically stacked mudrock deposits of dominantly grey-green-black coloration (95% Mudrock Facies Group 1) and sandy crevasse-splay deposits (S1.6). Most deposits are tabular; however, there are also some scour surfaces filled with brown to dark grey mudrock (M1.3).	A combination of compound to composite paleosols and erosion surfaces indicating rapid and unsteady floodplain sedimentation (sensu. Marriott and Wright 1993; Kraus 1999). Crevasse-splay deposits indicate channel migration by avulsion. The grey-green-black coloring of the facies suggests wet and reduced soils.
FA 5 Variably drained Floodplain Lithosomes	M1.3; M1.4; M1.5; M2.1; M2.2; M2.3; S1.6	Vertically stacked mudrock deposits of alternating grey-green (46% Mudrock Facies Group 1) and purple-red (22% Mudrock Facies Group 2) coloration and sandy crevasse-splay deposits (S1.6). Nearly all deposits are tabular.	Composite paleosols indicating unsteady floodplain deposition (sensu. Kraus 1999). Crevasse-splay deposits indicate channel migration by avulsion. The combination of grey-green (reduced) and purple-red (oxidized) paleosols suggests alternating wet and dry periods on the floodplain during times of slow deposition.
FA 6 Well drained Floodplain Lithosomes	M2.1; M2.2; M2.3; M1.3; M1.5; S1.6	Vertically stacked mudrock deposits with a high occurrence of purple-red coloration (42% Mudrock Facies Group 2) and sandy crevasse-splay deposits (S1.6). Nearly all of the deposits are tabular.	A combination of cumulative and compound paleosols indicating alterations between steady sedimentation and rapid, unsteady sedimentation (sensu. Krauss, 1999). Crevasse-splay deposits indicate channel migration by avulsion. The abundance of purple-red (oxidized) paleosols and the reduced occurence of drab (reduced) paleosols indicates that the floodplain was well drained and frequently dry.

(M2.2), and highly varicolored (gray-green, yellow-brown, purple, and red mottling, M2.3). Nearly all of the deposits are tabular, and scour surfaces truncating paleosol profiles are rarely observed unless they are associated with sandy channel fills.

Facies Association 5 Interpretation.—The development of purple-red deposits is attributed to the presence of hematite, an iron oxide mineral resulting from the soil being moderately to well drained and oxidizing (Retallack 1988). Purple mudrock deposits are interpreted as having weaker hematite impregnation compared to red mudrock deposits (Kraus et al. 2013). The mottles observed in these purple-red mudrock deposits are redoximorphic features produced by soil gleying and indicate that the soils were episodically saturated (Farnham and Kraus 2002). Furthermore, the presence of slickensides indicates repeated shrinking and swelling of clays due to fluctuations in the water table or seasonal wet–dry cycles at the surface (e.g., Bigham et al. 2002; Kraus and Riggins 2007). The combination of gleyed (reduced) and purple-red (oxidized) paleosols may indicate alternating wet and dry periods on the floodplain during times of low deposition rates or topographic variations in soil drainage conditions.

The vertically stacked mudrock deposits indicate a sedimentary system undergoing net aggradation. The presence of more strongly developed

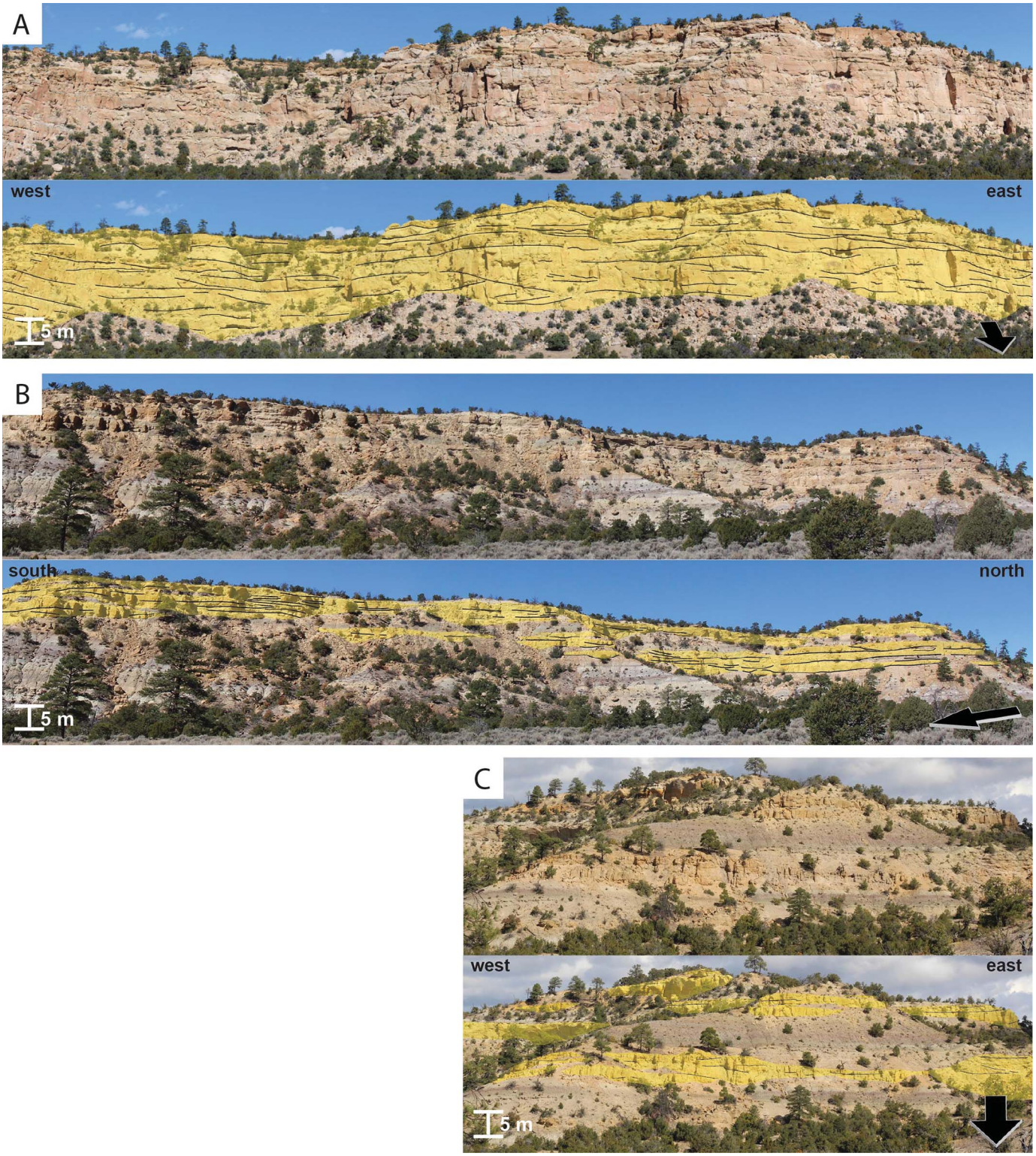

FIG. 8.—Examples of sandstone lithosomes. **A)** Sandy channel lithosomes (FA 1). **B)** Heterolithic channel lithosomes (FA 2). **C)** Lenticular channel lithosomes (FA 3). Paleoflow directions are indicated by the black arrows in lower right corner of annotated images.

peds, increased slickensides, increased mottling, and fewer mudrocks lacking visible pedogenic modification (compared to FA 4), combined with a lack of truncated paleosol profiles, indicates that erosion was insignificant, and sedimentation was unsteady enough to allow for paleosol development (*sensu* composite paleosols of Kraus 1999). The presence of interbedded poorly cemented, buff sandy deposits, interpreted as crevasse splays (see FA 4 interpretation), indicates that avulsion events were occurring on the floodplain.

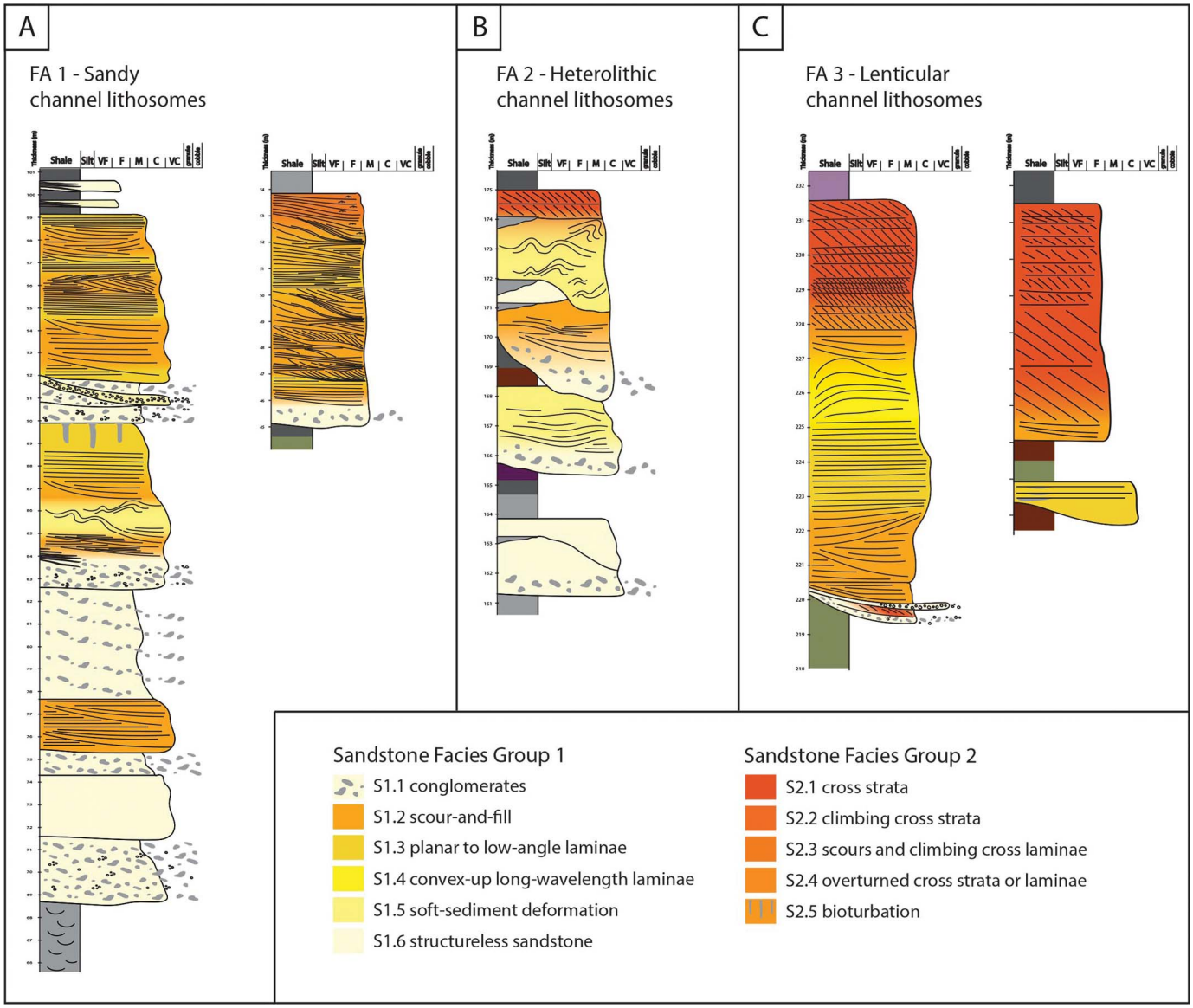

FIG. 9.—Representative measured sections and photos from sandstone lithosomes. **A)** Sandy channel lithosomes (FA 1). **B)** Heterolithic channel lithosomes (FA 2). **C)** Lenticular channel lithosomes (FA 3).

Facies Association 6 (FA 6): Well-Drained Floodplain Lithosomes

Facies association 6 consists of vertically stacked deposits with a high occurrence of purple-red mudrock (mudrock facies group 2, 42%), including purple mudrock (M2.1), red mudrock (M2.2), and mudrock with variegated color (M2.3) (Fig. 7C). Vertical successions of this facies association consist of alternations of thick (> 1 m), tabular mudrock layers exhibiting blocky to wedge-shaped peds, abundant slickensides, mottling, and carbonate nodules with thick deposits of mudrock lacking visible evidence of pedogenic modification (M1.3 and some deposits of M1.5, 30%) and thin (< 1 m) tabular or lenticular, and poorly cemented buff-colored sandy deposits (S1.6, 28%). These sandy deposits are difficult to distinguish from the surrounding mudrock facies because all of them display a similar style of badland erosion, forming steep slopes (> 45°) that are commonly capped with the well-cemented, cliff-forming sandstone channel deposits. Nearly all the deposits are tabular, and scour surfaces truncating paleosol profiles are not observed unless they are associated with sandy channel fill.

Facies Association 6 Interpretation.—The dominance of purple-red (oxidized) paleosols and a lack of gleyed (reduced) deposits indicates that the floodplain was well drained and frequently dry during times of low deposition. The wedge-shaped peds that are common in these deposits are thought to form only in soil profiles where seasonal precipitation and abundant fine clay combine to induce shrink–swell processes (Tabor et al. 2017). The presence of slickensides and mottles also indicates that the soils were episodically saturated. Carbonate nodules are formed under well drained, oxidizing conditions with a net water deficit due to evapotranspiration, and their presence indicates periods of dryness (Breecker et al. 2009). The combination of visible peds, abundant slickensides, mottling, and carbonate nodules in mudrock horizons measuring > 1 m in thickness is interpreted as strongly developed paleosol profiles (Tabor et al. 2017). Deposits with laminae, preserved organic matter, and/or a high silt content are interpreted as sediments devoid of visible pedogenic modification. In these cases, the deposits were likely buried before significant pedogenesis could take place (Tabor et al. 2017).

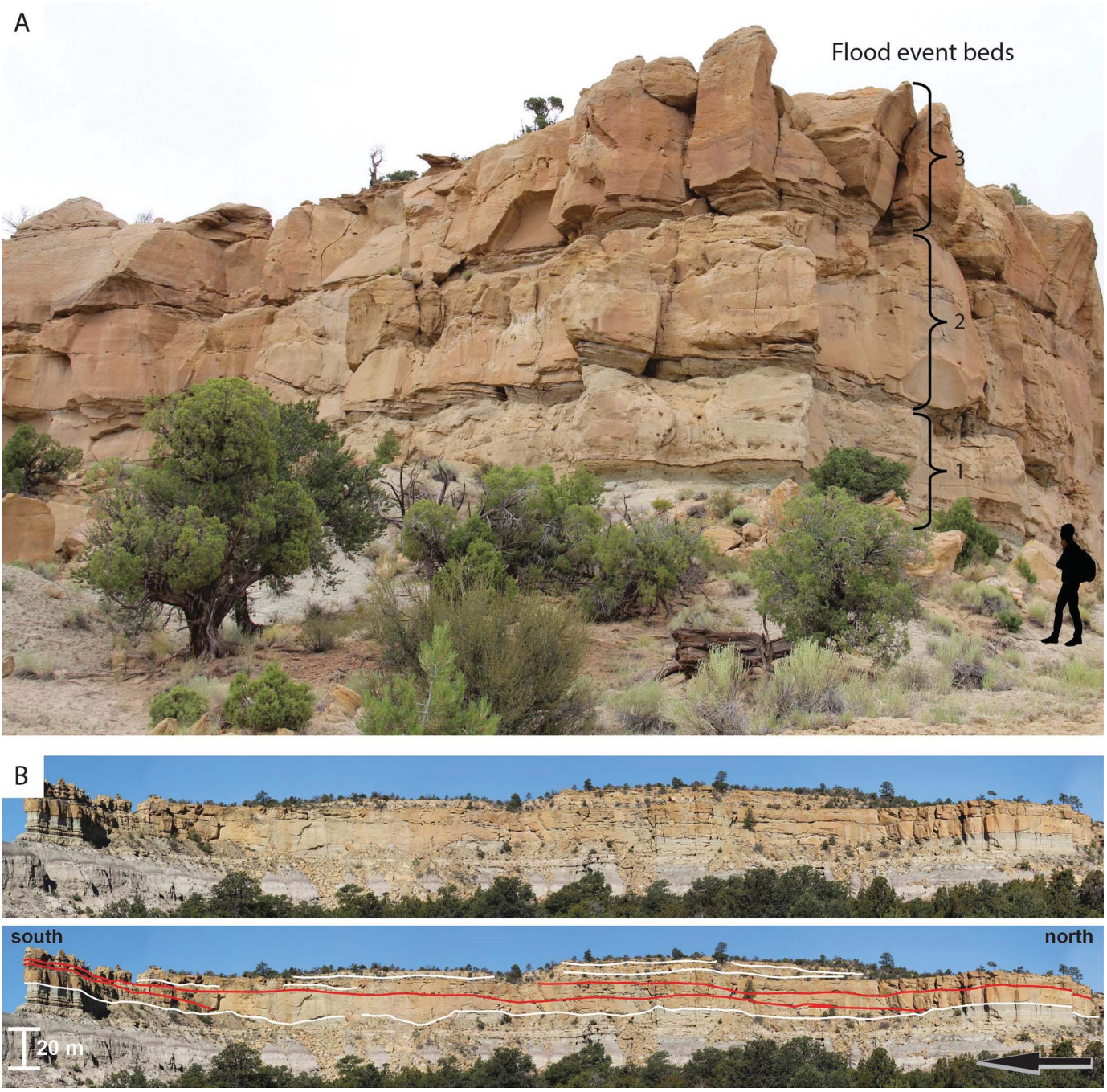

FIG. 10.—FA 1 channel characteristics. **A)** Three stacked, thick, and erosionally bounded sandstones interpreted as flood event beds separated by mud-clast conglomerates. Human scale (black silhouette in lower-right corner) is 1.8 m in height. **B)** FA 1 Channel with low-angle, upstream-dipping accretion sets. **C)** FA 1 channel consisting with annotated sedimentary facies **D)** Mud-clast conglomerates (S1.1) overlain by sandstone with low-angle laminae (S1.3). **E)** In-channel bioturbation (vertical burrows) is seen in the lower sandstone deposit, whereas the overlying deposit is not bioturbated and contains visible laminae. Paleoflow directions are indicated by the black arrows in annotated images.

As with FA 4 and FA 5, this facies association indicates a sedimentary system undergoing net aggradation. However, the alternation of thick, strongly developed paleosol profiles (*sensu* cumulative paleosols of Kraus 1999), mudrock deposits lacking visible pedogenic modification, and sandy deposits (*sensu* compound paleosols of Kraus 1999) indicate alternations between steady sedimentation and rapid, unsteady sedimentation. The weakly developed paleosols and mudrock deposits lacking visible pedogenic modification are commonly associated with sandy avulsion deposits. The presence of interbedded poorly cemented, buff sandy deposits, interpreted as crevasse splays (see FA 4 interpretation), also indicates that avulsion events were occurring on the floodplain. Taken together, the combination of facies in this association indicates periods of net aggradation through high deposition rates alternating with times of landscape stability in a frequently dry depositional environment.

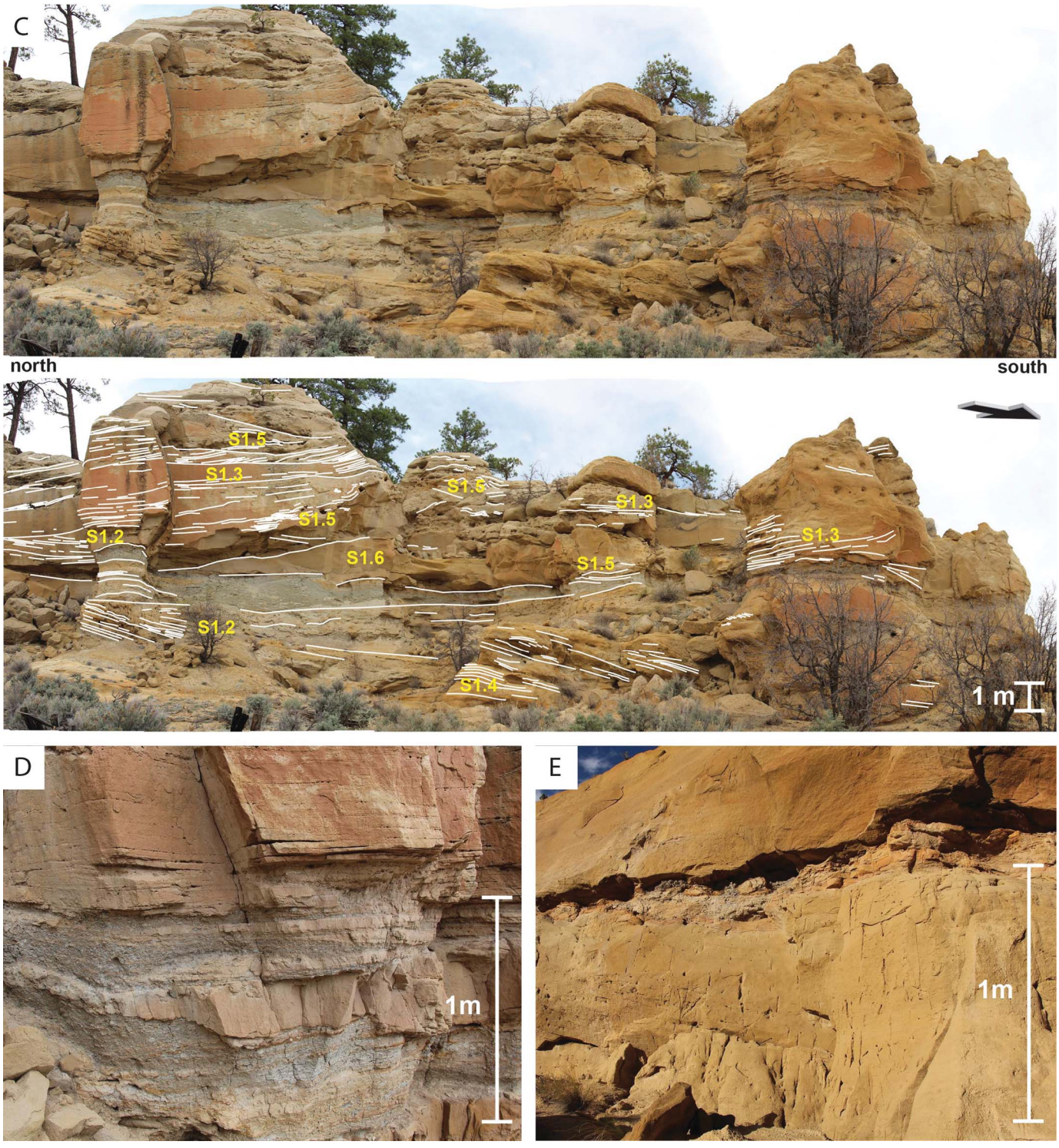

FIG. 10.—Continued.

DISCUSSION

Signatures of Variable Discharge in Channel Deposits and Comparison to Facies Models

The FAs 1–3 channel deposits are identified as deposits of variable-discharge river systems, based on a combination of 1) an abundance of UFR and HDR sedimentary structures indicative of high-magnitude flood events, 2) preservation of in-channel bioturbation and pedogenic modification indicating periods of prolonged dryness, 3) in-channel mudrock layers associated with high mud concentrations and rapidly waning flow, and 4) lack of identifiable braid-bar or point-bar strata characteristic of the upper flow regime. The proportion of UFR structures varies from dominant (96% and 89% in FAs 1 and 2, respectively) to

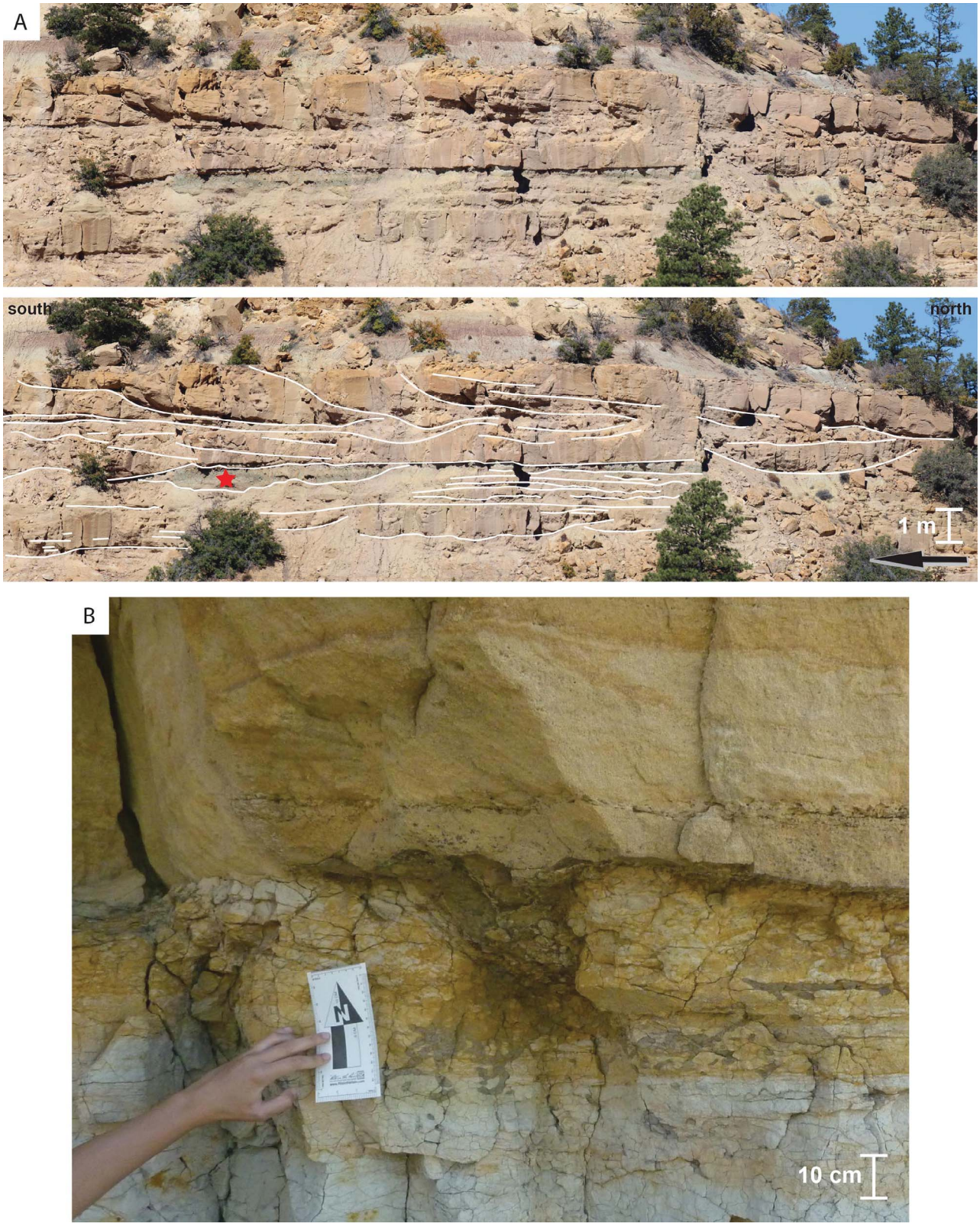

FIG. 11.—FA 2 channel characteristics. **A)** Heterolithic channel lithosome with pedogenic modification of in-channel mud layer at a downstream-dipping accretion boundary (marked with red star). The lower part of the lithosome displays low-angle downstream-accretion sets and the upper part erosionally bounded upstream-accretion sets. **B)** In-channel bioturbation in FA 2 channel fill. Paleoflow direction is indicated by the black arrow in lower right corner of annotated image.

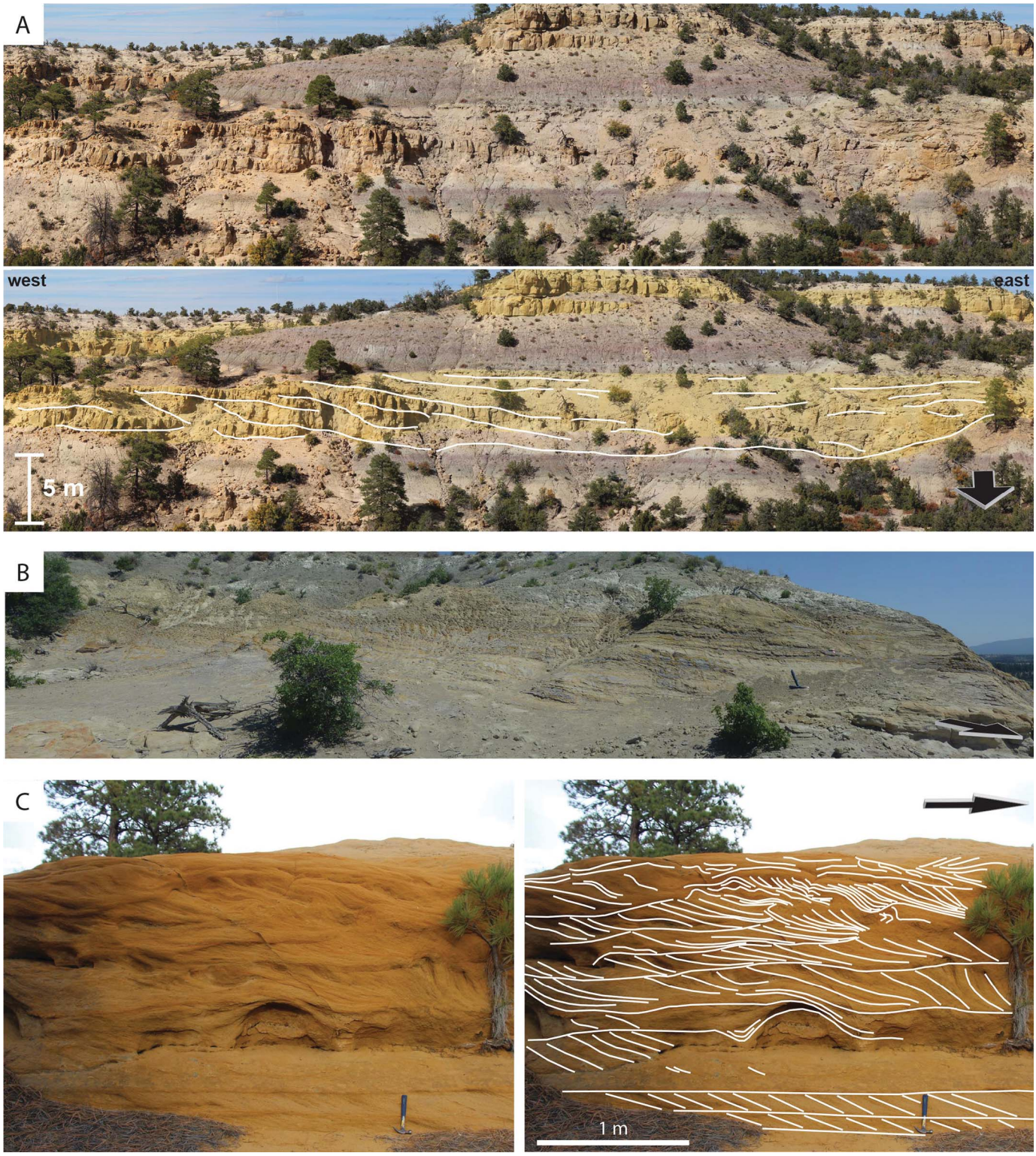

FIG. 12.—FA 3 channel characteristics. **A)** Lenticular channel with a channel-scale scour-and-fill structure with upward-flattening sets. **B)** Lenticular channel with mud layers separating sandy strata. **C)** Lenticular channel filled entirely with LFR structures from sandstone facies group 2 including cross strata and overturned cross strata. Paleoflow directions are indicated by the black arrows in lower right corner of annotated images.

abundant (50% in FA 3). The proportion of HDR structures remains dominant in all channel lithosomes. At macroform scale, the channel lithosomes display upstream or downstream accretion or channel-scale scour-and-fill structures where accretion sets are composed of flood event beds. Current facies models for deposits of variable-discharge rivers are primarily based on meso-scale sedimentary structures, as very few studies have systematically described macro-scale architecture other than noting that recognizable braid-bar or point-bar strata are missing or rare. Below, we compare to the proposed facies models for variable-discharge river deposits (Fielding et al. 2009, 2011, 2018; Plink-Björklund 2015, 2019) and to modern examples where possible.

FA 1 lithosomes share many characteristics with those described as amalgamated lithosomes with thick flood units in Plink-Björklund (2015), in that they consist of 80–100% of UFR and HDR sedimentary structures, lack in-channel mudrocks, consist of relatively thick flood event beds, and form lithosomes with a massive or uniform appearance in laterally and vertically amalgamated tabular sandstones (see also Tunbridge 1981; Stear 1985; Billi 2007). Thick mud-clast conglomerates and in-channel long vertical burrows have also been documented, and such lithosomes have been suggested to resemble flash-flood and megaflood deposits (e.g., Schumm 1961; McKee et al. 1967; Williams 1971; Stear 1985; Billi 2007; Plink-Björklund 2015; Fielding et al. 2018). On the macroform scale, the similarity includes low-angle downstream accretion (Plink-Björklund 2015; Wang and Plink-Björklund 2020). Modern river deposits with similar facies characteristics have been documented in the Kobo Basin, Ethiopia (Billi 2007), the Sinai Peninsula (Sneh 1983), and the Karoo in South Africa (Stear 1985). Mean annual precipitation varies considerably in these three areas from 750 mm in the former to $<$ 100 mm in the two latter areas. The similarities in climate include sustained droughts that last for most of a year (Billi 2007) to decades (Sneh 1983; Stear 1985), and that the whole annual precipitation falls in a few downpours that last from hours to a few days. Based on these characteristics, Plink-Björklund (2015) hypothesized that such channel lithosomes occur where intermittent intense rainfall, together with sparse vegetation, promote flash floods, high erosion rates, and high sediment flux. Plink-Björklund (2019) further speculated that such conditions may be characteristic for arid and semiarid subtropics with intermittent rainfall and lack of prolonged wet seasons.

FA 1 lithosomes also share some characteristics with the alluvial bodies with very high discharge variance proposed by Fielding et al. (2018). Similarities include a dominance of the same styles of UFR sedimentary structures (see also Fielding et al. 2009, 2011). Differences include macroform-scale architecture that is present and a lack of trees and sedimentary structures generated by in-channel vegetation (see also Fielding et al. 2009, 2011). Fielding et al. (2009, 2018) propose the Burdekin River (Fielding and Alexander 1996; Alexander and Fielding 1997; Alexander et al. 1999a, 1999b, 2001; Fielding et al. 1997, 1999; Nakayama et al. 2002; Amos et al. 2004) and the Fitzroy Rivers (e.g., Amos et al. 2008; Croke et al. 2011) of seasonal tropical northeast Australia, and Bijou Creek, Colorado (McKee et al. 1967) of the semiarid continental western USA, as modern analogues. They relate this depositional style to highly flashy discharge regimes and extreme interannual variability, where moderate or more intense rain tends to produce rapid runoff with a short response time, leading to highly peaked discharge hydrographs, especially in conditions of sparse vegetation following a prolonged drought.

FA 2 lithosomes are not well represented in the proposed facies models in that they are dominated by UFR and HDR sedimentary structures, contain in-channel mudrocks, and display downstream- and upstream-accretion sets. The exception is Wang and Plink-Björklund (2020) where similar strata are described in the Uinta Basin, Utah. However, in-channel mudrocks are documented from numerous modern and ancient settings (Williams 1971; Tunbridge 1981; Sneh 1983; Stear 1985; Abdullatif 1989; Olsen 1989; Singh and Bhardwaj 1991; Singh et al. 1993; North and Taylor 1996; Shukla et al. 2001; Billi 2007; Nichols and Fisher 2007; Fisher et al. 2008; Fielding et al. 2009, 2011, 2018; Chakraborty and Ghosh 2010; Allen et al. 2011; Mader and Redfern 2011; Plink-Björklund 2015, 2019; Wang and Plink-Björklund 2020). The listed modern examples occur in arid to subhumid subtropics, and in the monsoon zone. Thus, the presence of mud layers does not seem to be linked to a specific climate condition, and is rather linked to high mud concentrations and a rapid decline of floods (Plink-Björklund 2015), and perhaps the downstream position along a river length (Wang and Plink-Björklund 2019).

FA 3 lithosomes are most similar to the lithosomes with flood units and lower-flow-regime deposits of Plink-Björklund (2015) in that they contain around 50% UFR deposits and occasional lateral-accretion sets. Modern examples range from monsoonal-domain rivers (e.g., Shukla et al. 2001; Singh et al. 2007), to semiarid subtropics with mean annual precipitation of only 100–150 mm (Abdullatif 1989). This style of mixed UFR and LFR has been linked to rivers that transmit effective discharge for a whole wet season that lasts 3–5 months, and thus experience high- as well as low-magnitude floods (Abdullatif 1989; Plink-Björklund 2015, 2019). Peak discharges with high flow velocities and sediment concentrations, and thus deposition of UFR/HDR sedimentary structures, may last for only a few days and alternate with longer periods of lower discharge (Abdullatif 1989).

FA 3 is also similar to the alluvial deposits with intermediate-discharge-variance of Fielding et al. (2018) in that they report a mixture of UFR and LFR deposits. They do not, however, provide quantitative facies proportions. The proposed modern analogues with documented sedimentary records are the Eel River of northern California (Sloan et al. 2001) and the sandy, braided Platte River of Nebraska (Horn et al. 2012), central USA.

In summary, the proposed facies models suggest that FA 1 is linked to very flashy discharge that is likely to occur in arid, semiarid, and even subhumid tropical and subtropical climates with prolonged droughts, little vegetation, and intense intermittent rainfall. In contrast, multiple climatic regimes can be proposed for mixed UFR and LFR river systems of FA 3, ranging from arid to monsoonal systems with pronounced summer wet seasons to the winter-wet seasonal climate of California. Based on the provided examples, a common denominator seems to be the presence of a prolonged wet season, in contrast to the intense intermittent rainfall producing strata of FA 1 (see also Plink-Björklund 2019). FA 2 channel deposits cannot be linked to a specific climate type. Thus, although FAs 1–3 can be identified as deposits of variable-discharge rivers; they are not linked to specific climate types based on channel facies associations alone. There is, however, a suggested link between lithosome types and precipitation patterns (intermittent vs. pronounced wet season) for FAs 1 and 3.

Signatures of Variable Discharge in Floodplain Deposits

In addition to evidence of variable-discharge river systems from channel deposits, the floodplain deposits display indicators of moisture fluctuations and varying deposition rates. The crevasse-splay deposits observed in FAs 4–6 are related to partial or full avulsions, which are commonly observed in modern seasonal river systems due to the frequent occurrence of flood events (Abdullatif 1989; Makaske 2001; Jain and Sinha 2003, 2004; Assine 2005; Billi 2007; Assine and Silva 2009; Sinha et al. 2009; Chakraborty and Ghosh 2010; Donselaar et al. 2013), where highly variable flood discharges and high sediment concentrations result in rapid channel-bed aggradation and resultant superelevation, which is a key threshold for avulsion occurrence (Bryant et al. 1995; Hajek and Edmonds 2014). The avulsions result in high deposition rates on the floodplain as evidenced by sandy crevasse-splay deposits paired vertically with weakly

developed compound paleosols and mudrocks lacking visible pedogenic modification.

The FAs 4–6 lithosomes show alternations of compound paleosols and mudrocks lacking visible pedogenic modification with more developed composite and/or cumulative paleosols, indicating that avulsions were episodic and punctuated by periods of slow deposition allowing for varying levels of pedogenic development. A lack of pedogenic modification and weakly developed paleosols ("protosols") have also been linked to climatic conditions that inhibit or slow down pedogenesis, such as extreme aridity or cold (Kraus 1999). The coloration of the sediment and pedogenic features such as mottles, structure, and nodules in floodplain deposits can provide additional important information about climate and/or soil drainage conditions (e.g., Kraus and Hasiotis 2006; Vepraskas 2016). The most apparent evidence for highly variable soil moisture conditions is seen in the variably drained floodplain lithosome (FA 5), where the gleyed (reduced) deposits of mudrock facies group 1 are observed alternating with the purple-red (oxidized) deposits of mudrock facies group 2. However, some indicators of moisture fluctuations are present in all the floodplain lithosomes observed throughout the study interval, even those identified as lithosomes of poorly drained floodplains. These indicators include features like slickensides and wedge-shaped peds that indicate repeated shrinking and swelling of clays (Tabor et al. 2017). We suggest that these common features indicate that a signature of variable precipitation is present throughout the upper Nacimiento and San Jose formations, further supporting the evidence from channel systems. However, some additional indicators of variable precipitation such as carbonate nodules and more strongly developed ped structures are observed only in association with the variably drained and well-drained floodplain lithosomes (FA 5 and FA 6). It is important to note that our interpretations of the paleosols are based on qualitative assessments of texture and color. Including a detailed paleopedological investigation in future work would enable a quantitative estimate of paleoclimate conditions.

Channel–Floodplain Associations and Their Link to Hydroclimate

In order to further test hypotheses on the link between climate and the various styles of channel and floodplain deposits, we here combine evidence from channel and floodplain deposits. Six styles of channel–floodplain associations occur at different stratigraphic intervals: isolated lenticular channels (FA 3) in association with poorly drained floodplain deposits (FA 4) (Fig. 13A) and heterolithic channels (FA2) in association with poorly drained floodplain deposits (FA 4) (Fig. 13B) occur together in the Escavada Member. Amalgamated sandy channels (FA 1) in association with variably drained floodplain deposits (FA 5) (Fig. 13C) occur in the lower Cuba Mesa Member and heterolithic channels (FA 2) in association with variably drained floodplain deposits (FA 5) (Fig. 13D) occur in the middle and upper Cuba Mesa Member. Isolated channels (FA 3) occur in association with well-drained floodplain deposits (FA 6) in the lower Regina Member (Fig. 13E), and amalgamated channels (FA 1) occur in association with well-drained floodplain deposits (FA 6) in the upper Regina Member (Fig. 13F). The variety of associations implies multiple interesting perspectives on hydroclimate controls.

The combination of heterolithic channels (FA 2) and isolated channels (FA 3) in the same stratigraphic interval (Escavada Member) suggests that is unlikely that they are related to different precipitation regimes. This co-occurrence further suggests that these lithosome types may occur along the same rivers (see also Wang and Plink-Björklund 2019). Analyses of downstream changes in river discharge patterns, using data from multiple gauging stations along the same river, reveal that while the average discharge variability does not decrease downstream, the instantaneous effects of single storms (flashiness) do decrease (Hansford and Plink-Björklund 2020). Such a decrease in flashiness may be responsible for a downstream change in lithosome style. Nevertheless, the association of these variable-discharge channel lithosomes with the poorly drained floodplain lithosome (FA 4) suggests that wet conditions were relatively sustained, similar to modern monsoon climates. These channel–floodplain associations contradict the facies model proposed by Fielding et al. (2018), where monsoonal river deposits are hypothesized to be dominated by cross strata and support the hypothesis that they are more similar to river deposits in arid to humid subtropics (e.g., Kumar 1993; Singh et al. 1993; Willis 1993; Shukla et al. 2001; Chakraborty et al. 2010; Plink-Björklund 2015, 2019). The occurrence of FA 1 and FA 2 channel lithosomes in the Cuba Mesa Member may similarly reflect a downstream change (see Wang and Plink-Björklund 2019), such as preferential upstream sand deposition and downstream mud deposition. However, their association with variably drained floodplain deposits (FA 5) suggests a climate that had both considerable seasonal to interannual as well as decadal or longer precipitation variability that may be similar to modern subhumid tropical climates. The co-occurrence of FA 3 with well-drained floodplain lithosomes (FA 6) in the lower Regina Member contradicts suggestions that such isolated lenticular channel lithosomes are linked to monsoonal-domain rivers that experience a sustained wet season and transport perennial base flow, as was hypothesized by Plink-Björklund (2015). Instead, this channel–floodplain association may also develop at lower-magnitude precipitation events and/or losses due to evaporation and infiltration under more arid conditions and increased soil drainage (see Babcock and Cushing 1942; Ibrahim 1980; McCarthy and Ellery 1998). This style of precipitation variability is seen in some modern semiarid to arid subtropics, or drylands, that are characterized by high, yet variable, aridity, reflecting low precipitation totals and high evapotranspiration potential (see Tooth et al. 2013). The co-occurrence of FA 1 with FA 6 in the upper Regina Member suggests a dominantly arid environment and intense precipitation events resulting in high-magnitude flooding. This style of precipitation regime is also within the range of diversity observed in the modern semiarid to arid subtropics, or drylands (Tooth et al. 2013).

The observed diversity and overlap in channel–floodplain associations agrees with suggestions that tropical monsoonal, subtropical, and dryland subtropical rivers show many overlapping characteristics when the full range of river styles is considered in the climate zones (e.g., Knighton and Nanson 1997; Tooth and Nanson 2000; Powell 2009; see also review in Tooth et al. 2013). The findings that amalgamated sandy channels (FA 1) are associated with variably drained floodplain deposits (FA 5) and well-drained floodplain deposits (FA 6), heterolithic channels (FA 2) are associated with poorly drained floodplain deposits (FA 4) and variably drained floodplain deposits (FA 5), and, in particular, isolated lenticular channels (FA 3) are associated with both poorly (FA 4) and well-drained floodplain (FA 6) deposits strongly cautions simplistic use of variable-discharge channel lithosomes as proxies for paleoclimate or even hydroclimate types. These findings signify the importance of incorporating multiple data types, such as the combination of channel lithosomes and floodplain characteristics documented herein. Factors such as downstream variability along the river system must also be considered when analyzing datasets.

Evidence of Paleogene Climate Changes in the San Juan Basin

The fluvial deposits of the Escavada Member of the Paleocene Nacimiento Formation through the early Eocene Cuba Mesa and Regina members of the San Jose Formation show characteristics that suggest a range of variable precipitation regimes analogous to those of the modern monsoon and subtropical domains. Here, we discuss what these similarities and the stratigraphic positions of the various channel–floodplain associations may imply about Paleogene climate changes in the San Juan Basin.

The floodplain deposits suggest an overall trend of increasing aridity from the Paleocene into the early Eocene, but the diversity in the channel

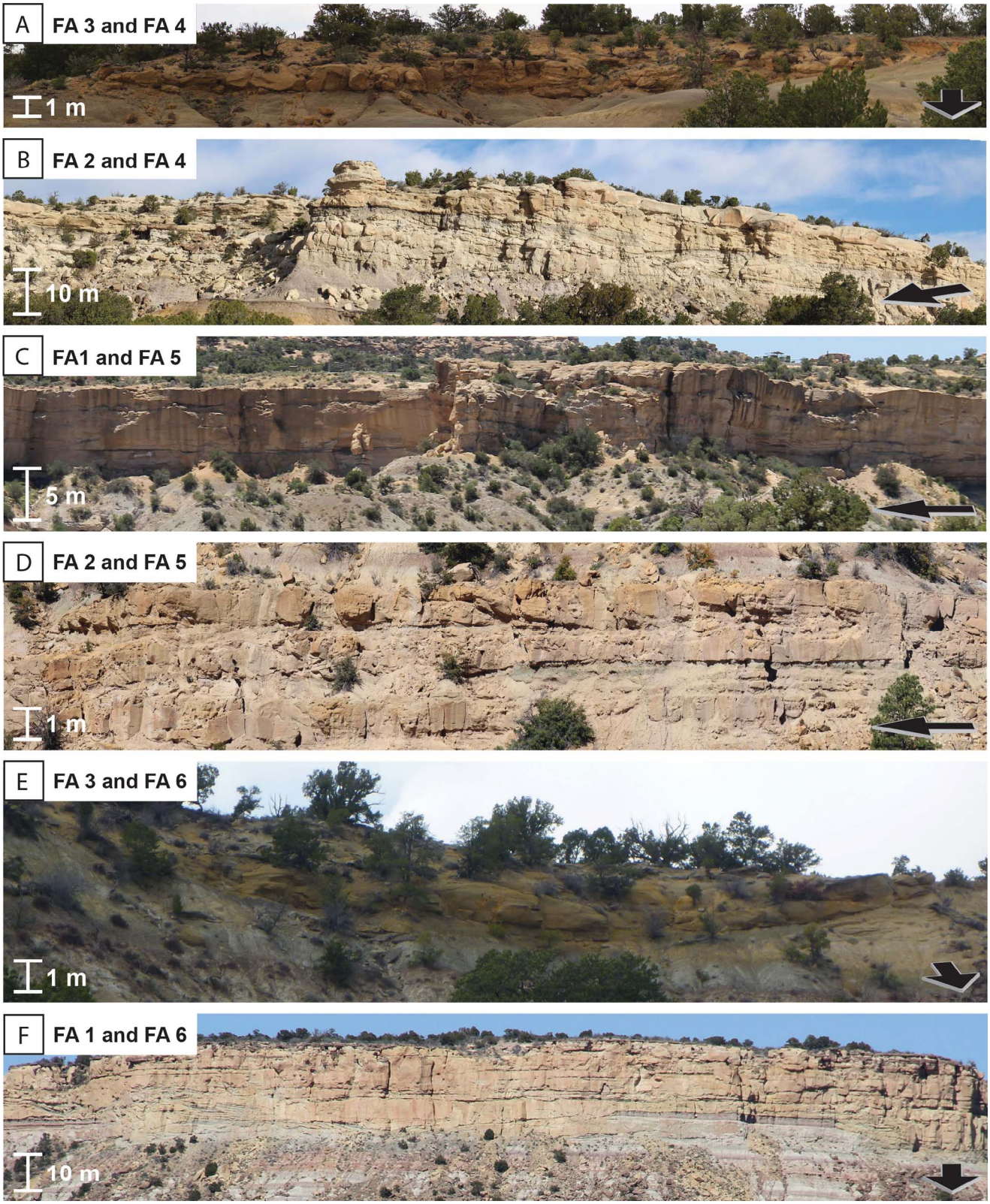

FIG. 13.—Examples of channel–floodplain associations. **A)** Lenticular channel lithosome (FA 3) in association with poorly drained floodplain lithosome (FA 4). **B)** Heterolithic channel lithosome (FA 2) in association with poorly drained floodplain lithosome (FA 4). **C)** Sandy channel lithosome (FA 1) in association with variably drained floodplain lithosome (FA 5). **D)** Heterolithic channel lithosome (FA 2) in association with variably drained floodplain lithosome (FA 5). **E)** Lenticular channel lithosome (FA 3) in association with well-drained floodplain lithosome (FA 6). **F)** Sandy channel lithosome (FA 1) in association with well-drained floodplain lithosome (FA 6). Paleoflow directions are indicated by the black arrows in the lower right corner of images.

lithosome styles suggests that considerable variability in the frequency and magnitude of precipitation and flooding events is superimposed on the long-term drying trend (Fig. 14). Furthermore, the stratigraphic clustering of the channel lithosome styles, as well as the stratigraphic variability in gleyed vs. purple-red paleosols, suggests some long-term trends, and perhaps cyclicity, in the frequency and magnitude of intense precipitation events. Wang et al. (2014, 2017) have shown that variability in modern monsoons and Quaternary paleo-monsoons occurs across time scales, from interannual, interdecadal, centennial, millennial, and up to orbital and tectonic timescales. The current lack of time constraints throughout the San Juan Basin study interval precludes further analysis of the frequency and duration of changes in the hydrological cycle, but the deposits in the study interval suggest multiple time scales of precipitation variability. In addition, some of the stratigraphic trends observed among the channel lithosomes may show evidence of threshold climate change beyond inherent monsoon precipitation variability. For example, the basin-wide FA 1 channel belt at the base of the Cuba Mesa Member, which corresponds with a shift from poorly drained (FA 4) to variably-drained (FA 5) floodplain deposits, may have resulted from sediment flushing as the ambient climate of the region shifted from a monsoonal precipitation regime in the Paleocene to variably subhumid and arid in the early Eocene (Fig. 14A). Reduction in vegetative cover, erosion of soils, and an increase in sediment yield is likely to result in a sediment flush under these conditions (Cecil and Dulong 2003). It is also suggested that once weathering and pedogenic equilibrium are reestablished under the drier conditions, rivers continue to show a relatively high solid-sediment yield (Cecil and Dulong 2003), which may be evidenced in the overlying FA 1 (central San Juan Basin) and FA 2 (southern San Juan Basin, Fig. 14B) channel lithosomes in the middle and upper Cuba Mesa Member. The return of FA 3 channels in the lower Regina Member could indicate decreased discharge and solid-sediment yield as the climate became increasingly arid, as suggested by their association with well-drained FA 6 floodplain deposits (Fig. 14C). However, the FA 1 channels in the upper Regina Member, which are also found in association with FA 6 floodplain deposits, suggest that rainfall intensity rather than overall aridity is a key control on water discharge and sediment yields.

The long-term trend towards increasing aridity observed in the floodplain deposits coincides with a global long-term warming trend from the Paleocene to the middle early Eocene upon which transient hyperthermals were superimposed (Zachos et al. 2008; Bijl et al. 2013). Huber and Goldner (2012) suggest that the intensity and distribution of precipitation changed as a result of the Paleogene warming trend, with greater moisture transport to high latitudes (Pagani et al. 2006) and enhanced seasonal extremes in some areas (John et al. 2008). In addition, it has been suggested that extremes in the hydrological cycle resulting in increased precipitation peakedness in the subtropics and mid-latitudes coincided with the Eocene hyperthermals (McInerney and Wing 2011; Plink-Björklund et al. 2014; Carmichael et al. 2016, 2018). The Paleocene and early Eocene deposits in the study interval suggest an overall long-term decrease in mean annual precipitation and fluctuations in seasonal extremes of precipitation and seem to suggest that floodplain deposits may be a better indicator of ambient climate, whereas channel deposits are records for frequency and magnitude of high-intensity precipitation events.

The long-term drying trend indicated by the San Juan Basin floodplain deposits differs from what has been suggested from records in other mid-latitude sedimentary basins with Paleocene–Eocene boundary deposits. In the Bighorn Basin, Wyoming, a transient decrease in precipitation has been suggested coincident with the Paleocene–Eocene Thermal Maximum (PETM) hyperthermal event (Kraus and Riggins 2007; Kraus et al. 2015). These researchers have also observed indicators of wet–dry cycles in the PETM interval floodplain deposits that they suggest may correspond to precessional cycles. The PETM interval is followed by indicators of similar to slightly wetter background soil moisture, using the CALMAG mean annual precipitation proxy, linked to four younger hyperthermal events (Abels et al. 2015). In the Uinta Basin, Utah, paleosol characteristics and trace fossils similarly suggest a transient shift to overall drier conditions during the PETM, followed by a wetter period with seasonally variable conditions (Golab 2010). In contrast, conditions in the Piceance Creek Basin, Colorado, are suggested to have been drier in the late Paleocene and more humid during the PETM due to an observed shift from a mix of purple, orange, and red paleosols to dominantly purple paleosols (Foreman et al. 2012). An abundance of red-pink paleosols above the identified PETM interval suggests drier conditions further into the early Eocene. In the Tremp–Graus Basin, Spain, semiarid conditions across the Paleocene–Eocene boundary are suggested, with an increase in intra-annual humidity gradients and associated seasonal flash floods during the PETM, followed by drier conditions immediately after the PETM (Schmitz and Pujalte 2007).

CONCLUSIONS

This study identifies the river and floodplain deposits of the Paleocene upper Nacimiento Formation (Escavada Member) through the Cuba Mesa and Regina members of the San Jose Formation in the San Juan Basin as formed by variable-discharge river systems, resulting from interannual (seasonal) and intra-annual precipitation variability. Evidence for a variable precipitation signature includes:

1. An abundance of upper-flow-regime sedimentary structures deposited under Froude supercritical flow conditions and high deposition rates in the channel deposits. A high percentage of upper-flow-regime and high-deposition-rate structures is characteristic of modern and ancient monsoonal and subtropical rivers that have highly seasonal discharge and receive most of their annual (or in some cases, interannual) precipitation from one to few large downpours resulting in flooding events.
2. Preservation of in-channel bioturbation and mud layers with pedogenic modification indicating that channels underwent periods of prolonged dryness between flooding episodes.
3. Floodplain lithosomes with alternations of poorly drained and more well-drained deposits and/or slickensides indicating alternating wet–dry cycles.
4. Floodplain lithosomes with crevasse-splay deposits that suggest channel avulsions resulting from flooding events.

Floodplain paleosols also evidence an overall long-term decrease in mean annual precipitation, whereas channel lithosomes reflect more short-term fluctuations in seasonal extremes of precipitation. Thus, integrating paleo-precipitation proxies from the river channel and floodplain deposits suggests that floodplain deposits may be a better indicator of ambient climate, whereas channel deposits are records for frequency and magnitude of high-intensity precipitation events. These data further suggest that the long-term drying trend that coincides with a long-term global warming trend from the Paleocene into the middle early Eocene was superimposed by fluctuations in hydrological-cycle extremes.

We show that when analyzed together and compared with precipitation variability from modern climate zones, the changes in channel–floodplain associations suggest a shift from a monsoonal precipitation regime in the Escavada Member of the Paleocene Nacimiento Formation to fluctuating subhumid and arid subtropical in the Cuba Mesa Member and semiarid to arid in the Regina Member of the early Eocene San Jose Formation.

We conclude that the existing facies models for variable-discharge rivers that consider only channel deposit facies may not capture critical information needed to make accurate interpretations of paleoclimatic conditions.

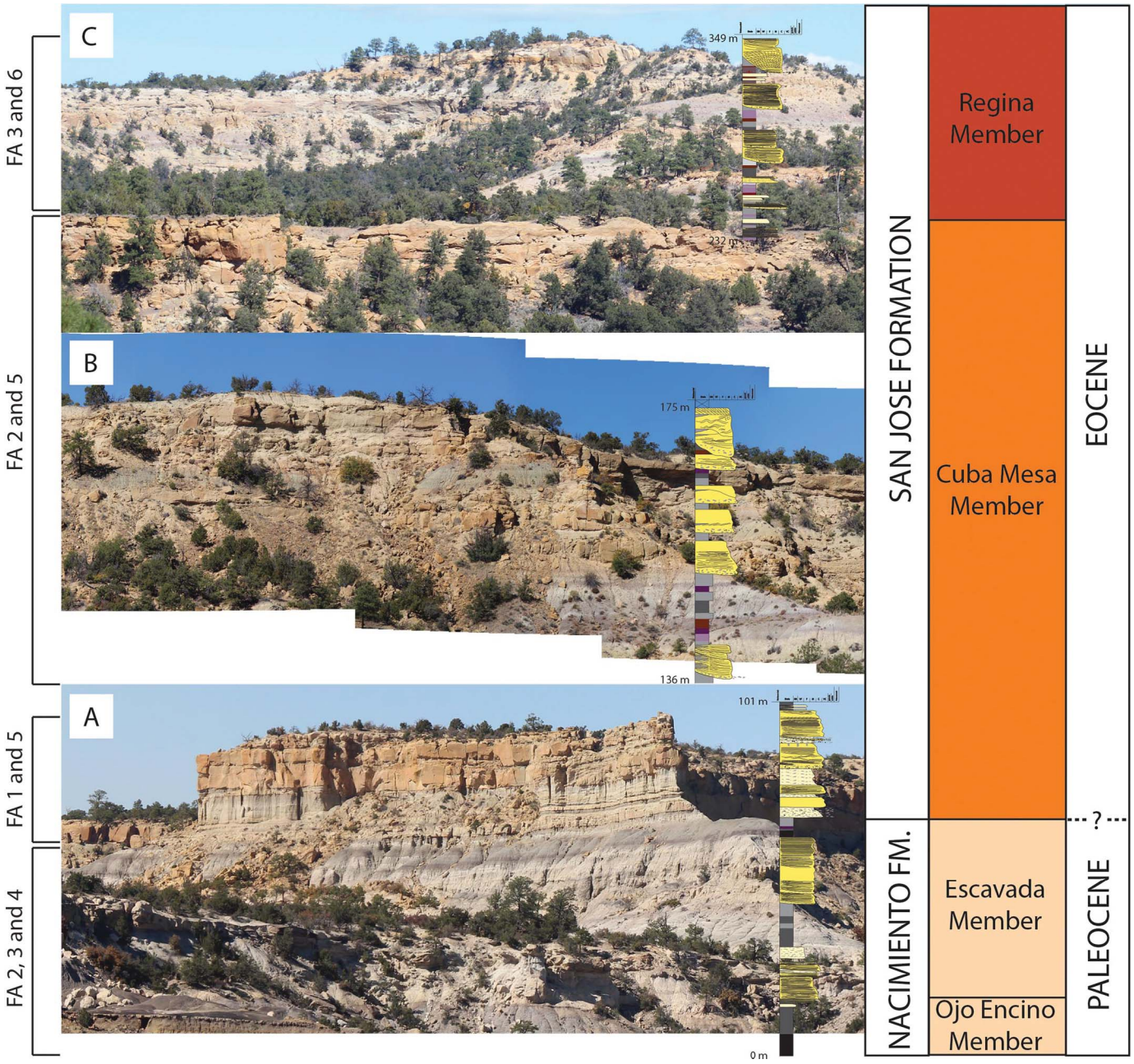

FIG. 14.—Stratigraphic trends in channel–floodplain associations in the Arroyo Chijuilla study area. Formation/Member names, locations of unit contacts, and generalized ages are shown to the right of the photo panels. **A)** Heterolithic channel lithosomes (FA 2) and lenticular channel lithosomes (FA 3) in association with poorly drained floodplain lithosomes (FA 4) in the uppermost Nacimiento Formation, capped by amalgamated sandy channel lithosomes (FA 1) in association with variably drained floodplain lithosomes (FA 5) in the lower Cuba Mesa channel complex. **B)** Heterolithic channel lithosomes (FA 2) in the middle Cuba Mesa channel complex in association with variably drained floodplain lithosomes (FA 5). **C)** Upper Cuba Mesa channel complex (FA 2) in association with variably drained floodplain lithosomes (FA 5) and overlying lenticular channel lithosomes (FA 3) in association with well-drained floodplain lithosomes (FA 6) in the Regina Member.

ACKNOWLEDGMENTS

We gratefully acknowledge Dr. Daniel Muhs, Associate Editor Dr. Alessandro Ielpi, Dr. Massimiliano Ghinassi, and an anonymous reviewer for constructive reviews of this article. Dr. Donna Anderson also provided a valuable review for an earlier version of this manuscript. We also thank Dr. Jianqiao Wang, Dessy Sapardina, Ariel Rickel, Leland Spangler, and Eric Miller for assistance during field work. Any use of trade, firm, or product names is for descriptive purposes only and does not imply endorsement by the U.S. Government.

REFERENCES

ABDULLATIF, O.M., 1989, Channel-fill and sheet-flood facies sequences in the ephemeral terminal River Gash, Kassala, Sudan: Sedimentary Geology, v. 63, p. 171–184.

ABELS, H.A., LAURETANO, V., VAN YPEREN, A., HOPMAN, T., ZACHOS, J.C., LOURENS, L.J., GINGERICH, P.D., AND BOWEN, G.J., 2015, Carbon isotope excursions in paleosol carbonate marking five early Eocene hyperthermals in the Bighorn Basin, Wyoming: Climate of the Past Discussions, v. 11, p. 1857–1885.

ALEXANDER, J.P., AND FIELDING, C.R., 1997, Gravel antidunes in the tropical Burdekin River, Queensland, Australia: Sedimentology, v. 44, p. 327–337.

Alexander, J., Bridge, J.S., Cheel, R.J., and Leclair, S.F., 2001, Bedforms and associated sedimentary structures formed under supercritical water flows over aggrading sand beds: Sedimentology, v. 48, p. 133–152.

Alexander, J.P., Fielding, C.R., and Pocock, G.D., 1999a, Flood behaviour of the Burdekin River, tropical north Queensland, Australia: Geological Society of London, Special Publication 163, p. 27–40.

Alexander, J.P., Fielding, C.R., and Jenkins, G., 1999b, Plant-material deposition in the tropical Burdekin River, Australia: implications for ancient fluvial sediments: Palaeogeography, Palaeoclimatology, Palaeoecology, v. 153, p. 105–125.

Allen, J.P., Fielding, C.R., Gibling, M.R., and Rygel, M.C., 2011, Fluvial response to paleo-equatorial climate fluctuations during the late Paleozoic ice age: Geological Society of America, Bulletin, v. 123, p. 1524–1538.

Allen, J.P., Fielding, C.R., Gibling, M.R., and Rygel, M.C., 2014, Recognizing products of palaeoclimate fluctuation in the fluvial stratigraphic record: an example from the Pennsylvanian to Lower Permian of Cape Breton Island, Nova Scotia: Sedimentology, v. 61, p. 1332–1381.

Allen, J.R.L., and Leeder, M.R., 1980, Criteria for the instability of upper-stage plane beds: Sedimentology, v. 27, p. 209–217.

Allen, P.A., 2008, From landscapes into geological history: Nature, v. 451, p. 274–276.

Amos, K.J., Alexander, J.P., Horn, A., Pocock, G.D., and Fielding, C.R., 2004, Supply limited sediment transport in a high-discharge event of the tropical Burdekin River, North Queensland, Australia: Sedimentology, v. 51, p. 145–162.

Amos, K.J., Croke, J.C., Hughes, A.O., Chapman, J., Takken, I., and Lymburner, L., 2008, A catchment-scale assessment of anabranching in the 143,000 km^2 Fitzroy River catchment, north-eastern Australia: Earth Surface Processes and Landforms, v. 33, p. 1222–1241.

Armitage, J.J., Duller, R.A., Whittaker, A.C., and Allen, P.A., 2011, Transformation of tectonic and climatic signals from source to sedimentary archive: Nature Geoscience. v. 4, p. 231–235.

Assine, M.L., 2005, River avulsions on the Taquari megafan, Pantanal wetland, Brazil: Geomorphology, v. 70, p. 357–371.

Assine, M.L., and Silva, A., 2009, Contrasting fluvial styles of the Paraguay River in the northwestern border of the Pantanal wetland, Brazil: Geomorphology, v. 113, p. 189–199.

Babcock, H.M., and Cushing, E.M., 1942, Recharge to ground-water from floods in a typical desert wash, Pinal County, Arizona: American Geophysical Union, Transactions, v. 23, p. 49–56.

Baltz, E.H., 1967, Stratigraphy and regional tectonic implications of part of Upper Cretaceous and Tertiary rocks, east-central San Juan Basin, New Mexico: U.S. Geological Survey, Professional Paper 552, 101 p.

Barnes, H., Baltz, E., Jr., and Hayes, P., 1954, Geology and fuel resources of the Red Mesa area, La Plata and Montezuma Counties, Colorado: U.S. Geological Survey, Oil and Gas Investigations Map OM-149, scale 1:62,500.

Bigham, J.M., Fitzpatrick, R.W., and Schulze, D.G., 2002, Iron Oxides, *in* Dixon, J.B., and Schulze, D.G., eds., Soil Mineralogy with Environmental Applications: Soil Science Society of America, Book Series, p. 323–366.

Bijl, P.K., Bendle, J.A.P., Bohaty, S.M., and Pross, J., et al., 2013, Eocene cooling linked to early flow across the Tasmanian Gateway: National Academy of Sciences [USA], Proceedings, v. 110, p. 9645–9650.

Billi, P., 2007, Morphology and sediment dynamics of ephemeral stream terminal distributary systems in the Kobo Basin (northern Welo, Ethiopia): Geomorphology, v. 85, p. 98–113.

Birgenheier, L.P., Vanden Berg, M.D., Plink-Björklund, P., Gall, R.D., Rosencrans, E., Rosenberg, M.J., Toms, L.C., and Morris, J., 2020, Climate impact on fluvial–lake system evolution, Eocene Green River Formation, Uinta Basin, Utah, USA: Geological Society of America, Bulletin, v. 132, p. 562–587.

Breecker, D.O., Sharp, Z.D., and McFadden, L.D., 2009, Seasonal bias in the formation and stable isotopic composition of pedogenic carbonate in modern soils from central New Mexico, USA: Geological Society of America, Bulletin, v. 121, p. 630–640.

Bridge, J.S., 2003, Rivers and Floodplains: Forms, Processes, and Sedimentary Record: Blackwell, Oxford, 504 p.

Bridge, J.S., and Best, J.L., 1997, Preservation of planar laminae due to migration of low-relief bed waves over aggrading upper-stage plane beds: comparison of experimental data with theory: Sedimentology, v. 44, p. 253–262.

Bridge, J.S., and Best, J.L., 1988, Flow, sediment transport and bedform dynamics over the transition from dunes to upper-stage plane beds: implications for the formation of planar laminae: Sedimentology, v. 35, p. 753–763.

Bridge, J.S., and Leeder, M.R., 1979, A simulation model of alluvial stratigraphy: Sedimentology, v. 26, p. 617–644.

Bridge, J.S., Alexandar, J.P., Collier, R.E.L., Gawthorpe, R.L., and Jarvis, J., 1995, Ground-penetrating radar and coring used to study the large-scale structure of point-bar deposits in three dimensions: Sedimentology, v. 42, p. 839–852.

Bryant, M., Falk, P., and Paola, C., 1995, Experimental study of avulsion frequency and rate of deposition: Geology, v. 23, p. 365–368.

Bull, W.B., 1991, Geomorphic Responses to Climatic Change: Oxford University Press, 326 p.

Bull, W.B., 2009, Tectonically Active Landscapes: Wiley-Blackwell, 320 p.

Butler, R.F., and Lindsay, E.H., 1985, Mineralogy of magnetic minerals and revised magnetic polarity stratigraphy of continental sediments, San Juan Basin, New Mexico: The Journal of Geology, v. 93, p. 535–554.

Carmichael, M.J., Lunt, D.J., Huber, M., Heinemann, M., Kiehl, J., LeGrande, A., Loptson, C.A., Roberts, C.D., Sagoo, N., Shields, C., Valdes, P.J., Winguth, A., Winguth, C., and Pancost, R.D., 2016, A model–model and data–model comparison for the early Eocene hydrological cycle: Climate of the Past, v. 12, p. 455–481.

Carmichael, M.J., Pancost, R.D., and Lunt, D.J., 2018, Changes in the occurrence of extreme precipitation events at the Paleocene–Eocene thermal maximum: Earth and Planetary Science Letters, v. 501, p. 24–36.

Cartigny, M.J.B., Ventra, D., Postma, G., and van Den Berg, J.H., 2014, Morphodynamics and sedimentary structures of bedforms under supercritical-flow conditions: new insights from flume experiments: Sedimentology, v. 61, p. 712–748.

Cather, S.M., 2004, Laramide orogeny in central and northern New Mexico and southern Colorado, *in* Mack, G., and Giles, K., eds., The Geology of New Mexico, A Geologic History: New Mexico Geological Society, Special Publication 11, p. 203–248.

Cecil, C.B., and Dulong, F., 2003, Precipitation models for sediment supply in warm climates, *in* Cecil, C.B., and Edgar, T., eds., Climate Controls on Stratigraphy: SEPM, Special Publication 77, p. 21–28.

Cecil, C.B., Dulong, F.T., West, R., Stamm, R., Wardlaw, B., and Edgar, T., 2003, Climate controls on the stratigraphy of a Middle Pennsylvanian cyclothem in North America, *in* Cecil, C.B., and Edgar, T., eds., Climate Controls on Stratigraphy, SEPM, Special Publication 77, p. 151–182.

Chakraborty, T., and Ghosh, P., 2010, The geomorphology and sedimentology of the Tista megafan, Darjeeling Himalaya: implications for megafan building processes: Geomorphology, v. 115, p. 252–266.

Chakraborty, T., Kar, R., Ghosh, P., and Basu, S., 2010, Kosi megafan: historical records, geomorphology and the recent avulsion of the Kosi River: Quaternary International, v. 227, p. 143–160.

Cheel, R.J., 1986, Horizontal laminae formed under upper-flow regime plane bed conditions: The Journal of Geology, v. 94, p. 489–504.

Coleman, J.M., 1969, Brahmaputra river: channel processes and sedimentation: Sedimentary Geology, v. 3, p. 129–239.

Croke, J., Jansen, J.D., Amos, K., and Pietsch, T.J., 2011, A 100 ka record of fluvial activity in the Fitzroy River Basin, tropical northeastern Australia: Quaternary Science Reviews, v. 30, p. 1681–1695.

Deluca, J.L., and Eriksson, K.A., 1989, Controls on synchronous ephemeral, and perennial-river sedimentation in the middle sandstone member of the Triassic Chinle Formation, northeastern New Mexico, U.S.A.: Sedimentary Geology, v. 61, p. 155–175.

DiBiase, R.A., and Whipple, K.X., 2011, The influence of erosion thresholds and runoff variability on the relationships among topography, climate, and erosion rate: Journal of Geophysical Research, v. 116, p. 1–17.

Dickinson, W.R., Klute, M.A., Hayes, M.J., Janecke, S.U., Lundin, E.R., McKittrick, M.A., and Olivares, M.D., 1988, Paleogeographic and paleotectonic setting of Laramide sedimentary basins in the central Rocky Mountain region: Geological Society of America, Bulletin, v. 100, p. 1023–1039.

Donselaar, M.E., Cuevas Gozalo, M.C., and Moyano, S., 2013, Avulsion processes at the terminus of low-gradient semiarid fluvial systems: lessons from the Río Colorado, Altiplano endorheic basin, Bolivia: Sedimentary Geology, v. 283, p. 1–14.

Duller, R.A., Whittaker, A.C., Fedele, J.J., Whitchurch, A.L., Springett, J., Smithells, R., Fordyce, S., and Allen, P.A., 2010, From grain size to tectonics: Journal of Geophysical Research, Earth Surface, v. 115, F03022.

Farnham, T.M., and Kraus, M.J., 2002, The stratigraphic and climatic significance of Paleogene alluvial paleosols in synorogenic strata of the Denver Basin, Colorado: Rocky Mountain Geology, v. 37, p. 201–213.

Fassett, J.E., 1985, Early Tertiary paleogeography and paleotectonics of the San Juan basin area, New Mexico and Colorado, *in* Flores, R.M., and Kaplan, S.S., eds., Cenozoic Paleogeography of the West-Central United States: SEPM, Rocky Mountain Section, p. 317–334.

Fassett, J., Heizler, M., and McIntosh, W., 2010, Geologic implications of an $^{40}Ar/^{39}Ar$ single-crystal sanidine age for an altered volcanic ash bed in the Paleocene Nacimiento Formation in the southern San Juan Basin, *in* Fassett J.E., Zeigler, K.E., and Lueth, V., eds., Geology of the Four Corners Country: New Mexico Geological Society, 61st Annual Field Conference Guidebook, p. 147–156.

Fielding, C.R., 2006, Upper-flow regime sheets, lenses and scour fills: extending the range of architectural elements for fluvial sediment bodies: Sedimentary Geology, v. 190, p. 227–240.

Fielding, C.R., and Alexander, J., 1996, Sedimentology of the upper Burdekin River of North Queensland, Australia: an example of a tropical, variable discharge river: Terra Nova, v. 8, p. 447–457.

Fielding, C.R., Alexander, J., and Newman-Sutherland, E., 1997, Preservation of in situ, arborescent vegetation and fluvial bar construction in the Burdekin River of north Queensland, Australia: Palaeogeography, Palaeoclimatology, Palaeoecology, v. 135, p. 123–144.

Fielding, C., Alexander, J., McDonald, R., Smith, N., and Rogers, J., 1999, Sedimentary facies from ground-penetrating radar surveys of the modern, upper Burdekin River of north Queensland, Australia: consequences of extreme discharge fluctuations, *in* Smith, N.D., and Rogers, J., eds., Fluvial Sedimentology VI: International Association of Sedimentologists, Special Publication 28, p. 347–362.

Fielding, C.R., Allen, J.P., Alexander, J., and Gibling, M.R., 2009, Facies model for fluvial systems in the seasonal tropics and subtropics: Geology, v. 37, p. 623–626.
Fielding, C.R., Allen, J.P., Gibling, M.R., and Rygel, M.C., 2011, Fluvial response to paleo-equatorial climate fluctuations during the late Paleozoic ice age: Geological Society of America, Bulletin v. 123, p. 1524–1538.
Fielding, C.R., Alexander, J., and Allen, J.P., 2018, The role of discharge variability in the formation and preservation of alluvial sediment bodies: Sedimentary Geology, v. 365, p. 1–20.
Fisher, J.A., Krapf, C.B.E., Lang, S.C., Nichols, G.J., and Payenberg, T.H.D., 2008, Sedimentology and architecture of the Douglas Creek terminal splay, Lake Eyre, central Australia: Sedimentology, v. 55, p. 1915–1930.
Foreman, B.Z., 2014, Climate-driven generation of a fluvial sheet sand body at the Paleocene–Eocene boundary in north-west Wyoming (USA): Basin Research, v. 26, p. 225–241.
Foreman, B.Z., Heller, P.L., and Clementz, M.T., 2012, Fluvial response to abrupt global warming at the Palaeocene–Eocene boundary: Nature, v. 491, 92–95.
Frostick, L.E., and Reid, I., 1977, The origin of horizontal laminae in ephemeral stream channel-fill: Sedimentology, v. 24, p. 1–9.
Gingerich, P.D., 1989, New earliest Wasatchian mammalian fauna from the Eocene of northwestern Wyoming: composition and diversity in a rarely sampled high-floodplain assemblage: University of Michigan, Papers on Paleontology 28, 97 p.
Gohain, K., and Parkash, B., 1990, Morphology of the Kosi Megafan, *in* Rachocki, A.H., and Church, M., eds., Alluvial Fans: A Field Approach, Wiley, p. 151–178.
Golab, J.A., 2010, Ichno-Pedological Facies of the Colton and Lower-Middle Green River Formations: Implications for Continental Paleoclimate Studies [MS Thesis]: Colorado School of Mines, Golden, Colorado, 101 p.
Goodbred, S.L., 2003, Response of the Ganges dispersal system to climate change: a source-to-sink view since the last interstade: Sedimentary Geology, v. 162, p. 83–104.
Graf, W.L., 1988, Fluvial Processes in Dryland Rivers: Springer-Verlag, 346 p.
Hajek, E.A., and Edmonds, D.A., 2014, Is river avulsion style controlled by floodplain morphodynamics?: Geology, v. 42, p. 199–202.
Hampton, B.A., and Horton, B.K., 2007, Sheetflow fluvial processes in a rapidly subsiding basin, Altiplano plateau, Bolivia: Sedimentology, v. 54, p. 1121–1148.
Hansford, M.R., and Plink-Björklund, P., 2020, River discharge variability as the link between climate and fluvial fan formation: Geology, v. 48, p. 1–5.
Hansford, M.R., Plink-Björklund, P., and Jones, E.R., 2020, Global quantitative analyses of river discharge variability and hydrograph shape with respect to climate types: Earth-Science Reviews, v. 200, p. 1–20.
Hasiotis, S.T., Kraus, M.J., and Demko, T.M., 2007, Climatic controls on continental trace fossils, *in* Miller, W., ed., Trace Fossils: Elsevier, p. 172–195.
Henck, A.C., Montgomery, D.R., Huntington, K.W., and Liang, C., 2010, Monsoon control of effective discharge, Yunnan and Tibet: The Journal of Geology, v. 38, p. 975–978.
Horn, J.D., Joeckel, R.M., and Fielding, C.R., 2012, Progressive abandonment and planform changes of the central Platte River in Nebraska, central USA, over historical timeframes: Geomorphology, v. 139–140, p. 372–383.
Huber, M., and Goldner, A., 2012, Eocene monsoons: Journal of Asian Earth Sciences, v. 44, p. 3–23.
Hulka, C., and Heubeck, C., 2010, Composition and provenance history of late Cenozoic sediments in southeastern Bolivia: implications for Chaco foreland basin evolution and Andean uplift: Journal of Sedimentary Research, v. 80, p. 288–299.
Ibrahim, A., 1980, River Gash behaviour and training [MS Thesis]: University of Khartoum. 105 p.
IPCC, 2014, Climate Change 2014: Synthesis Report, Contribution of Working Groups I, II, and III to the Fifth Assessment Report of the Intergovernmental Panel on Climate Change, *in* Pachauri, R.K., and Meyer, L.A., eds., Intergovernmental Panel on Climate Change, 151 p.
Jain, V., and Sinha, R., 2003, Hyperavulsive-anabranching Baghmati river system, north Bihar plains, eastern India: Zeitschrift für Geomorphologie, v. 47, p. 101–116.
Jain, V., and Sinha, R., 2004, Fluvial dynamics of an anabranching river system in Himalayan foreland basin, Baghmati River, north Bihar plains, India: Geomorphology, v. 60, p. 147–170.
Jerolmack, D.J., and Paola, C., 2010, Shredding of environmental signals by sediment transport: Geophysical Research Letters, v. 37, p. 1–5.
John, C.M., Bohaty, S.M., Zachos, J.C., Sluijs, A., Gibbs, S., Brinkhuis, H., and Bralower, T.J., 2008, North American continental margin records of the Paleocene–Eocene thermal maximum: implications for global carbon and hydrological cycling: Paleoceanography and Paleoclimatology, v. 23, p. 1–20.
Jones, C.M., 1977, Effects of varying discharge regimes on bed-form sedimentary structures in modern rivers: Geology, v. 5, p. 567–570.
Jones, L.S., and Schumm, S.A., 1999, Causes of avulsion: an overview, *in* Smith, N.D., and Rogers, J., eds., Fluvial Sedimentology VI: International Association of Sedimentologists, Special Publication 28, p. 171–178.
Kale, V.S., Ely, L.L., Enzel, Y., and Baker, V.R., 1994, Geomorphic and hydrologic aspects of monsoon floods on the Narmada and Tapi rivers in central India: Proceedings of the 25th Binghamton Symposium in Geomorphology, Geomorphology and Natural Hazards, p. 157–168.
Karcz, I., 1969, Mud pebbles in a flash floods environment: Journal of Sedimentary Petrology, v. 39, p. 333–337.
Kennett, J.P., and Stott, L.D., 1991, Abrupt deep-sea warming, palaeoceanographic changes and benthic extinctions at the end of the Paleocene: Nature, v. 353, p. 225–229.
Klute, M.A., 1986, Sedimentology and sandstone petrography of the upper Kirtland Shale and Ojo Alamo Sandstone, Cretaceous–Tertiary boundary, western and southern San Juan Basin, New Mexico: American Journal of Science, v. 286, p. 463–488.
Knighton, A., and Nanson, G., 1997, Distinctiveness, diversity and uniqueness in arid zone river systems, *in* Thomas, D.S.G., ed., Arid Zone Geomorphology: Process, Form, and Change in Drylands: John Wiley & Sons, p. 185–203.
Koch, P.L., Zachos, J.C., and Gingerich, P.D., 1992, Correlation between isotope records in marine and continental carbon reservoirs near the Palaeocene–Eocene boundary: Nature, v. 358, p. 319–322.
Kraus, M.J., 1999, Paleosols in clastic sedimentary rocks: their geologic applications: Earth-Science Reviews, v. 47, p. 41–70.
Kraus, M.J., and Hasiotis, S.T., 2006, Significance of different modes of rhizolith preservation to interpreting paleoenvironmental and paleohydrologic settings: examples from Paleogene paleosols, Bighorn Basin, Wyoming, U.S.A.: Journal of Sedimentary Research, v. 76, p. 633–646.
Kraus, M.J., and Riggins, S., 2007, Transient drying during the Paleocene–Eocene Thermal Maximum (PETM): analysis of paleosols in the Bighorn Basin, Wyoming: Palaeogeography, Palaeoclimatology, Palaeoecology, v. 245, p. 444–461.
Kraus, M.J., McInerney, F.A., Wing, S.L., Secord, R., Baczynski, A.A., and Bloch, J.I., 2013, Paleohydrologic response to continental warming during the Paleocene–Eocene Thermal Maximum, Bighorn Basin, Wyoming: Palaeogeography, Palaeoclimatology, Palaeoecology, v. 370, p. 196–208.
Kraus, M.J., Woody, D.T., Smith, J.J., and Dukic, V., 2015, Alluvial response to the Paleocene–Eocene Thermal Maximum climatic event, Polecat Bench, Wyoming (U.S.A.): Palaeogeography, Palaeoclimatology, Palaeoecology, v. 435, p. 177–192.
Kumar, R., 1993, Goalescence megafan: multistorey sandstone complex of the late-orogenic (Mio-Pliocene) sub-Himalayan belt, Dehra, Dun, India: Sedimentary Geology, v. 85, p. 327–337.
Langbein, W.B., and Schumm, S.A., 1958, Yield of sediment in relation to mean annual precipitation: American Geophysical Union, Transactions, v. 39, 1076–1084.
Latrubesse, E.M., Stevaux, J.C., and Sinha, R., 2005, Tropical rivers: Geomorphology, v. 70, p. 187–206.
Laury, R.L., 1971, Stream bank failure and rotational slumping: preservation and significance in the geologic record: Geological Society of America, Bulletin, v. 82, p. 1251–1266.
Lawton, T.F., 2008, Laramide sedimentary basins, *in* Miall, A.D., ed., Sedimentary Basins of the United States and Canada: Elsevier, p. 429–450.
Leeder, M.R., 2011, Sedimentology and Sedimentary Basins: From Turbulence to Tectonics: Wiley-Blackwell, 784 p.
Leier, A.L., DeCelles, P.G., and Pelletier, J.D., 2005, Mountains, monsoons, and megafans: The Journal of Geology, v. 33, p. 289–292.
Leslie, C., Peppe, D., Williamson, T., Bilardello, D., Heizler, M., Secord, R., and Leggett, T., 2018, High-resolution magnetostratigraphy of the upper Nacimiento Formation, San Juan Basin, New Mexico, USA: implications for basin evolution and mammalian turnover: American Journal of Science, v. 318, p. 300–334.
Lucas, S.G., Manning, E., and Tsentas, C., 1981, The Eocene biostratigraphy of New Mexico: Geological Society of America, Bulletin, v. 92, p. 951–967.
Lunt, I.A., Bridge, J.S., and Tye, R.S., 2004, A quantitative, three-dimensional depositional model of gravelly braided rivers: Sedimentology, v. 51, p. 377–414.
Macklin, M.G., Lewin, J., and Woodward, J.C., 2012, The fluvial record of climate change: Royal Society of London, Philosophical Transactions, Mathematical, Physical and Engineering Sciences, v. 370, p. 2143–2172.
Mader, N.K., and Redfern, J., 2011, A sedimentological model for the continental Upper Triassic Tadrart Ouadou Sandstone Member: recording an interplay of climate and tectonics (Argana Valley; south-west Morocco): Sedimentology, v. 58, p. 1247–1282.
Makaske, B., 2001, Anastomosing rivers: a review of their classification, origin and sedimentary products: Earth-Science Reviews, v. 53, p. 149–196.
Manley, K., Scott, G.R., and Wobus, R.A., 1987, Geologic map of the Aztec quadrangle, northwestern New Mexico and southern Colorado: U.S. Geological Survey, Miscellaneous Investigations Series Map I-1730, scale 1:250,000.
Marriott, S.B., and Wright, P.V., 1993, The sequence stratigraphy of fluvial depositional systems: the role of floodplain sediment storage: Sedimentary Geology, v. 86, p. 203–210.
McCarthy, T.S., and Ellery, W.N., 1998, The Okavango Delta: Royal Society of South Africa, Transactions, v. 53, p. 157–182.
McInerney, F.A., and Wing, S.L., 2011, The Paleocene–Eocene Thermal Maximum: a perturbation of carbon cycle, climate, and biosphere with implications for the future: Annual Review of Earth and Planetary Sciences, v. 39, p. 489–516.
McKee, E.D., Crosby, E.J., and Berryhill, H.L., 1967, Flood deposits, Bijou Creek, Colorado: Journal of Sedimentary Petrology, v. 37, p. 829–851.
Mills, P.C., 1983, Genesis and diagnostic value of soft-sediment deformation structures: a review: Sedimentary Geology, v. 35, p. 83–104.
Molnar, P., Anderson, R.S., Kier, G., and Rose, J., 2006, Relationships among probability distributions of stream discharges in floods, climate, bed load transport, and river incision: Journal of Geophysical Research. v. 111. p. 1–10.

Mytton, J.W., 1983, Geologic map of Chaco Canyon 30′ × 60′ quadrangle showing coal zones of Fruitland Formation, San Juan, Rio Arriba, and Sandoval counties, New Mexico: U.S. Geological Survey, Coal Investigations Map C-92-A, scale 1:100,000.

Nakayama, K., Fielding, C.R., and Alexander, J., 2002, Variations in character and preservation potential of vegetation-induced obstacle marks in the variable discharge Burdekin River of north Queensland, Australia: Sedimentary Geology, v. 149, p. 199–218.

Naqshband, S., Hoitink, A.J.F., McElroy, B., Hurther, D., and Hulscher, S.J.M.H., 2017, A sharp view on river dune transition to upper stage plane bed: Geophysical Research Letters, v. 44, p. 11437–11444.

Nichols, G.J., and Fisher, J.A., 2007, Processes, facies and architecture of fluvial distributary system deposits: Sedimentary Geology, v. 195, p. 75–90.

North, C.P., and Taylor, K.S., 1996, Ephemeral-fluvial deposits: integrated outcrop and simulation studies reveal complexity: American Association of Petroleum Geologists, Bulletin, v. 80, p. 811–830.

Olsen, H., 1989, Sandstone-body structures and ephemeral stream processes in the Dinosaur Canyon Member, Moenave Formation (Lower Jurassic), Utah, U.S.A.: Sedimentary Geology, v. 61, p. 207–221.

Ono, K., Plink-Björklund, P., Eggenhuisen, J.T., and Cartigny, M.J.B., 2020, Froude supercritical flow processes and sedimentary structures: new insights from experiments with a wide range of grain sizes: Sedimentology, v. 2020, p. 1–30.

Pagani, M., Pedentchouk, N., Huber, M., and Sluijs, A., et al., and Expedition 302 Scientists, 2006, Arctic hydrology during global warming at the Palaeocene–Eocene thermal maximum: Nature, v. 442, p. 671–675.

Paola, C., Wiele, S.M., and Reinhart, M.A., 1989, Upper-regime parallel lamination as the result of turbulent sediment transport and low-amplitude bed forms: Sedimentology, v. 36, p. 47–59.

Pecha, M.E., Gehrels, G.E., Karlstrom, K.E., Dickinson, W.R., Donahue, M.S., Gonzales, D.A., and Blum, M.D., 2018, Provenance of Cretaceous through Eocene strata of the Four Corners region: insights from detrital zircons in the San Juan Basin, New Mexico and Colorado: Geosphere, v. 14, p. 785–811.

Peel, M.C., Finlayson, B.L., and McMahon, T.A., 2007, Updated world map of the Köppen–Geiger climate classification: Hydrology and Earth System Sciences, v. 11, p. 1633–1644.

Plink-Björklund, P., 2015, Morphodynamics of rivers strongly affected by monsoon precipitation: review of depositional style and forcing factors: Sedimentary Geology, v. 323, p. 110–147.

Plink-Björklund, P., 2019, Latitudinal controls on river systems: implications of precipitation variability, *in* Fraticelli, C.M., Markwick, P.J., Martinius, A.W., and Suter, J.R., eds., Latitudinal Controls on Stratigraphic Models and Sedimentary Concepts: SEPM, Special Publication 108. p. 59–81.

Plink-Björklund, P., Birgenheier, L., and Jones, E., 2014, Extremely bad early Eocene weather: evidence for extreme precipitation from river deposits: Società Geologica Italiana, Rendiconti online, v. 31, p. 175–176.

Postma, G., 2014, Generic autogenic behavior in fluvial systems: lessons from experimental studies, *in* Martinius, A.W., Ravnas, R., Howell, J.A., Steel, R.J., and Wonham, J.P., eds., From Depositional Systems to Sedimentary Successions on the Norwegian Continental Margin: International Association of Sedimentologists, Special Publication 46, p. 1–18.

Postma, G., and Cartigny, M.J.B., 2014, Supercritical and subcritical turbidity currents and their deposits: a synthesis: Geology, v. 42, p. 987–990.

Postma, G., Cartigny, M., and Kleverlaan, K., 2009, Structureless, coarse-tail graded Bouma Ta formed by internal hydraulic jump of the turbidity current?: Sedimentary Geology, v. 219, p. 1–6.

Powell, D.M., 2009, Dryland rivers: processes and forms, *in* Parsons, A.J., and Abrahams, A.D., eds., Geomorphology of Desert Environments: The Netherlands, Springer, p. 333–373.

Reid, I., and Frostick, L.E., 2011, Channel form, flows and sediments of endogenous ephemeral rivers in deserts, *in* Thomas, D.S.G., ed., Arid Zone Geomorphology: Process, Form and Change in Drylands: John Wiley & Sons, p. 301–332.

Retallack, G., 1988, Field recognition of paleosols, *in* Reinhardt, J., and Sigleo, W.R., eds., Paleosols and Weathering Through Geologic Time: Principles and Applications: Geological Society of America, Special Paper 216, p. 1–20.

Rhee, C.W., and Chough, S.K., 1993, The Cretaceous Pyonghae sequence, southeast Korea: terminal fan facies: Palaeogeography, Palaeoclimatology, Palaeoecology, v. 105, p. 139–156.

Ruhe, R.V., 1956, Geomorphic surfaces and the nature of soils: Soil Science, v. 82, p. 441–456.

Schmitz, B., and Pujalte, V., 2007, Abrupt increase in seasonal extreme precipitation at the Paleocene–Eocene boundary: Journal of Geology, v. 35, p. 215–218.

Schumm, S.A., 1961, Effect of sediment characteristics on erosion and deposition in ephemeral stream channels: U.S. Geological Survey, Professional Paper 352-C, 70 p.

Seneviratne, S.I., Nicholls, N., Easterling, D., and Goodess, C.M., et al., eds., Managing the Risks of Extreme Events and Disasters to Advance Climate Change Adaptation: Special Report of the Intergovernmental Panel on Climate Change: Cambridge University Press, p. 109–230.

Shukla, U.K., Singh, I.B., Sharma, M., and Sharma, S., 2001, A model of alluvial megafan sedimentation: Ganga Megafan: Sedimentary Geology, v. 144, p. 243–262.

Sikkink, P.G.L., 1987, Lithofacies relationships and depositional environment of the Tertiary Ojo Alamo Sandstone and related strata, San Juan Basin, New Mexico and Colorado, *in* Fassett, J.E., and Rigby, J.K., eds., The Cretaceous–Tertiary Boundary in the San Juan and Raton Basins, New Mexico and Colorado: Geological Society of America, Special Paper 209, p. 81–104.

Simpson, G.G., 1948, The Eocene of the San Juan Basin, New Mexico, Part 1: American Journal of Science, v. 246, p. 257–282.

Singh, A., and Bhardwaj, B.D., 1991, Fluvial facies model of the Ganga River sediments, India: Sedimentary Geology, v. 72, p. 135–146.

Singh, H., Parkash, B., and Gohain, K., 1993, Facies analysis of the Kosi megafan deposits: Sedimentary Geology, v. 85, p. 87–113.

Singh, M., Singh, I.B., and Müller, G., 2007, Sediment characteristics and transportation dynamics of the Ganga River: Geomorphology, v. 86, p. 144–175.

Sinha, R., Gibling, M.R., Tandon, S.K., Jain, M., Bhattacharjee, P.S., Dasgupta, A.S., and Ghazanfari, P., 2009, Craton-derived alluvium as a major sediment source in the Himalayan Foreland Basin of India: Geological Society of America, Bulletin, v. 121, p. 1596–1610.

Sloan, J., Miller, J.R., and Lancaster, N., 2001, Response and recovery of the Eel River, California, and its tributaries to floods in 1955, 1964, and 1997: Geomorphology, v. 36, p. 129–154.

Smith, L.N., 1988, Basin analysis of the lower Eocene San Jose Formation, San Juan Basin, New Mexico and Colorado [Ph.D. dissertation]: University of New Mexico, Albuquerque, 166 p.

Smith, L.N., 1992, Stratigraphy, sediment dispersal and paleogeography of the lower Eocene San Jose Formation, San Juan Basin, New Mexico and Colorado, *in* San Juan Basin IV: New Mexico Geological Society, 43rd Field Conference, Guidebook, p. 297–309.

Smith, L.N., and Lucas, S.G., 1991, Stratigraphy, sedimentology, and paleontology of the lower Eocene San Jose Formation in the central portion of the San Juan Basin, northwestern New Mexico: New Mexico Bureau of Mines and Mineral Resources, Bulletin 126, 44 p.

Sneh, A., 1983, Desert stream sequences in the Sinai Peninsula: Journal of Sedimentary Petrology, v. 53, p. 1271–1279.

Sólyom, P.B., and Tucker, G.E., 2004, Effect of limited storm duration on landscape evolution, drainage basin geometry, and hydrograph shapes: Journal of Geophysical Research, v. 109, p. 1–13.

Stear, W.M., 1985, Comparison of the bedform distribution and dynamics of modern and ancient sandy ephemeral flood deposits in the southwestern Karoo region, South Africa: Sedimentary Geology, v. 45, p. 209–230.

Stone, W.J., 1983, Hydrogeology and water resources of the San Juan Basin, New Mexico: New Mexico Bureau of Mines and Mineral Resources, Hydrologic Report 6, 70 p.

Syvitski, J.P.M., and Milliman, J.D., 2007, Geology, geography, and humans battle for dominance over the delivery of fluvial sediment to the coastal ocean: The Journal of Geology, v. 115, p. 1–19.

Syvitski, J.P.M., Cohen, S., Kettner, A.J., and Brakenridge, G.R., 2014, How important and different are tropical rivers?: an overview: Geomorphology, v. 227, p. 5–17.

Tabor, N.J., Myers, T.S., and Michel, L.A., 2017, Sedimentologist's guide for recognition, description, and classification of paleosols, *in* Zeigler, K.E., and Parker, W.G., eds., Terrestrial Depositional Systems: Deciphering Complexities through Multiple Stratigraphic Methods: Elsevier, p. 165–208.

Tandon, S.K., and Gibling, M.R., 1997, Calcretes at sequence boundaries in upper carboniferous cyclothems of the Sydney Basin, Atlantic Canada: Sedimentary Geology, v. 112, p. 43–67.

Thomas, E., 1989, Development of Cenozoic deep-sea benthic foraminiferal faunas in Antarctic waters: Geological Society of London, Special Publication 47, p. 283–296.

Tooth, S., 2000, Process, form and change in dryland rivers: a review of recent research: Earth-Science Reviews, v. 51, p. 67–107.

Tooth, S., and Nanson, G.C., 2000, The role of vegetation in the formation of anabranching channels in an ephemeral river, Northern plains, arid central Australia: Hydrological Processes, v. 14, p. 3099–3117.

Tooth, S., Brandt, D., Hancox, P.J., McCarthy, T.S., Jacobs, Z., and Woodborne, S., 2013, Controls on the genesis, sedimentary architecture, and preservation potential of dryland alluvial successions in stable continental interiors: insights from the incising Modder River, South Africa: Journal of Sedimentary Research, v. 83, p. 541–561.

Tucker, G.E., 2004, Drainage basin sensitivity to tectonic and climatic forcing: implications of a stochastic model for the role of entrainment and erosion thresholds: Earth Surface Processes and Landforms, v. 29, p. 185–205.

Tucker, G.E., 2009, Natural experiments in landscape evolution: Earth Surface Processes and Landforms, v. 34, p. 1450–1460.

Tunbridge, I.P., 1981, Sandy high-energy flood sedimentation: some criteria for recognition, with an example from the Devonian of S.W. England: Sedimentary Geology, v. 28, p. 79–95.

Uba, C., Heubeck, C., and Hulka, C., 2005, Facies analysis and basin architecture of the Neogene Subandean synorogenic wedge, southern Bolivia: Sedimentary Geology, v. 180, p. 91–123.

Vepraskas, M.J., 2016, Wetland Soils: Genesis, Hydrology, Landscapes, and Classification: CRC Press, Taylor & Francis Group, 495 p.

Wang, B., and Ding, Q., 2008, Global monsoon: dominant mode of annual variation in the tropics: Dynamics of Atmospheres and Oceans, v. 44, p. 165–183.

Wang, J., and Plink-Björklund, P., 2019, Stratigraphic complexity in fluvial fans: Lower Eocene Green River Formation, Uinta Basin, USA: Basin Research, v. 31, p. 892–919.
Wang, J., and Plink-Björklund, P., 2020, Variable-discharge-river macroforms in the Sunnyside Delta interval of the Eocene Green River Formation, Uinta Basin, USA: Sedimentology, v. 67, p. 1914–1950.
Wang, P.X., Wang, B., Cheng, H., Fasullo, J., Guo, Z.T., Kiefer, T., and Liu, Z.Y., 2014, The global monsoon across timescales: coherent variability of regional monsoons: Climate of the Past, v. 10, p. 2007–2052.
Wang, P.X., Wang, B., Cheng, H., Fasullo, J., Guo, Z., Kiefer, T., and Liu, Z., 2017, The global monsoon across time scales: mechanisms and outstanding issues: Earth-Science Reviews, v. 174, p. 84–121.
West, L.M., Perillo, M.M., and Steel, R.J., 2019, Multi-event organization of deepwater sediments into bedforms: long-lived, large-scale antidunes preserved in deepwater slopes: Geology, v. 47, p. 391–394.
Whipple, K.X., 2004, Bedrock rivers and the geomorphology of active orogens: Annual Review of Earth and Planetary Sciences, v. 32, p. 151–185.
Whipple, K.X., 2009, The influence of climate on the tectonic evolution of mountain belts: Nature Geoscience, v. 2, p. 97–104.
Whittaker, A.C., 2012, How do landscapes record tectonics and climate?: Lithosphere, v. 4, p. 160–164.
Whittaker, A.C., Attal, M., Cowie, P.A., Tucker, G.E., and Roberts, G., 2008, Decoding temporal and spatial patterns of fault uplift using transient river long profiles: Geomorphology, v. 100, p. 506–526.
Whittaker, A.C., Attal, M., and Allen, P.A., 2009, Characterising the origin, nature and fate of sediment exported from catchments perturbed by active tectonics: Basin Research, v. 22, p. 809–828.
Williams, G.E., 1971, Flood deposits of the sand-bed ephemeral streams of central Australia: Sedimentology, v. 17, p. 1–40.
Williamson, T.E., and Lucas, S.G., 1992, Stratigraphy and mammalian biostratigraphy of the Paleocene Nacimiento Formation, southern San Juan Basin, New Mexico, *in* San Juan Basin IV: New Mexico Geological Society, 43rd Field Conference, Guidebook, p. 265–296.
Williamson, T.E., Crossey, L.J., and Lucas, S.G., 1992, Silcretes of the Paleocene Nacimiento Formation, *in* San Juan Basin IV: New Mexico Geological Society, 43rd Field Conference, Guidebook, p. 38–46.
Williamson, T.E., Nichols, D.J., and Weil, A., 2008, Paleocene palynomorph assemblages from the Nacimiento Formation, San Juan Basin, New Mexico, and their biostratigraphic significance: New Mexico Geology, v. 30, p. 3–11.
Willis, I., 2005, Hydrology of glacierised basins, *in* Anderson, M.G., ed., Encyclopedia of Hydrological Sciences: Chichester, Wiley, p. 2601–2631.
Willis, B.J., 1993, Interpretation of bedding geometry within ancient point-bar deposits, *in* Marzo, M., and Puidefábregas C., eds., Alluvial Sedimentation: International Association of Sedimentologists, Special Publication 17, p. 101–114.
Wobus, C., Whipple, K.X., Kirby, E., Snyder, N., Johnson, J., Spyropolou, K., Crosby, B., and Sheehan, D., 2006a, Tectonics from topography: procedures, promise, and pitfalls, *in* Willett, S.D., Hovius, N., Brandon, M.T., and Fisher, D.M., eds., Tectonics, Climate, and Landscape Evolution: Geological Society of America, Special Paper 398, p. 55–74.
Wobus, C.W., Whipple, K.X., and Hodges, K.V., 2006b, Neotectonics of the central Nepalese Himalaya: constraints from geomorphology, detrital $^{40}Ar/^{39}Ar$ thermochronology, and thermal modeling: neotectonics of central Nepal: Tectonics, v. 25, p. 1–18.
Woodward, L.A., 1987, Geology and mineral resources of Sierra Nacimiento and vicinity, New Mexico: New Mexico Bureau of Mines and Mineral Resources, Memoir 42, 84 p.
Zachos, J., 2001, Trends, rhythms, and aberrations in global climate 65 Ma to present: Science, v. 292, p. 686–693.
Zachos, J.C., Dickens, G.R., and Zeebe, R.E., 2008, An early Cenozoic perspective on greenhouse warming and carbon-cycle dynamics: Nature, v. 451, p. 279–283.

Received 26 September 2019; accepted 18 October 2020.